

國立臺灣大學工學院化學工程學系



碩士論文

Department of Chemical Engineering

College of Engineering

National Taiwan University

Master Thesis

使用非耦合近似方法模擬反應中非諧振性及其在沸石系統中的應用

Modeling Anharmonicity in Reactions with Uncoupled Mode Approximations and Its Application in Zeolite Systems

林岩均

Yen-Chun Lin

指導教授：李奕霈 博士

Advisor: Yi-Pei Li, Ph.D.

中華民國 112 年 7 月

July, 2023



國立臺灣大學碩(博)士學位論文
口試委員會審定書

使用非耦合近似方法模擬反應中非諧振性
及其在沸石系統中的應用

Modeling Anharmonicity in Reactions with Uncoupled Mode
Approximations and Its Application in Zeolite Systems

本論文係林岩均君(學號 r10524074)在國立臺灣大學化學工程學系、所完成之碩(博)士學位論文，於民國 112 年 7 月 5 日承下列考試委員審查通過及口試及格，特此證明

口試委員：

李光弼 (簽名)
(指導教授)
林以 林祥泰
劉昭仁 林立強

系主任、所長

廖英志 (簽名)

(是否須簽章依各院系所規定)

誌謝



時間過的很快，兩年的實驗室生活一溜煙就過去了，在過程中有對無數次對自己研究生活的迷惘以及作業報告的壓力，但也有不少在解決問題後獲得的成就感以及忙裡偷閒的愉快時光。相信在未来的日子中，會很慶幸自己有踏入 N415 做研究學習，以及認識老師同學們。首先要先感謝李奕霈教授，在剛進入實驗室懵懵懂懂的時候總是能夠耐著性子推著我慢慢前進，同時鼓勵以及督導我能夠在研究的路上更盡心盡力，在我遇到問題的時候總是能提出相當精闢的見解與建議。接著要感謝世晟學長對我不厭其煩的教導，從一開始連程式碼都看不太懂，到後來能夠漸漸地跟上進度一起完成研究。再來也要感謝畢業的建毅學長，在我剛進入實驗室當專題生時教導我做量子力學計算的基本知識以及操作方法。同時，也必須要感謝實驗室所有同學的互相砥礪，總是能在遇到問題的時候互相交流以及排解壓力。最後，也必須要感謝我的家人默默地在背後支持著我，讓我能夠順利進入研究所，並且心無旁騖地專注在研究的生活中！

中文摘要



沸石已被廣泛應用於許多不同的領域，尤其是在石油精煉工業中。對具有不同孔隙結構和組成的沸石進行催化性能預測將具有很高的價值。然而，傳統的諧振子模型（Harmonic oscillator, HO）常常無法提供準確的熵或動力學性質計算，因為它忽略了非諧振性。為了解決這些問題，我們使用了考慮獨立一維非諧位能曲面總和的非耦合模式（Uncoupled mode, UM）方法。我們廣泛研究了包括 UM-N、UM-VT、UM-T、E-optimized 和 E'-optimized 等五種不同的位能曲面近似方法，發現 UM-VT 和 UM-T 在預測氣相分子系統的熱力學和動力學性質和實驗值有很好的一致性。我們還檢查了內座標系統的影響，發現相對於常見的內坐標（Redundant internal coordinate, RIC），使用移動-轉動-內坐標（Translation-rotation-internal coordinate, TRIC）系統和混合內坐標（Hybrid internal coordinate, HIC）系統可以更正確地計算動力學性質。將 TRIC 內部座標搭配 UM 方法應用於 H-MFI 沸石上的烷烴裂解反應，可以略微提高對內在活化熵（Intrinsic activation entropy）的估計，但還需要進一步的改進才能達到化學準確性。

關鍵字：熱力學、動力學、沸石、量子化學計算、催化

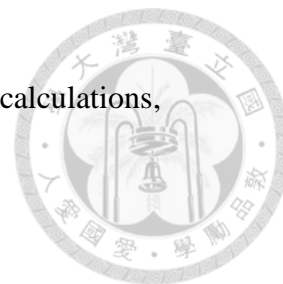
Abstract



Zeolites have been widely applied to many different fields, especially in oil refining industry. Prediction of catalytic performance for zeolites with different pore topologies and structure formations would be highly valuable. However, the conventional harmonic oscillator model often fails to provide accurate entropy or kinetic properties calculations due to the ignorance of anharmonic effects. To address these issues, we employed uncoupled mode (UM) methods that consider the sum of independent one-dimensional anharmonic potential energy surfaces. We extensively investigated five different potential energy surface sampling schemes including UM-N, UM-VT, UM-T, E-optimized, E'-optimized and found that UM-VT, and UM-T perform well in predicting thermodynamic and kinetic properties in gas phase molecular systems. We also examined the impact of internal coordinate systems, finding that translation-rotation-internal coordinate (TRIC) system and hybrid internal coordinate (HIC) system outperform redundant internal coordinates (RIC) for kinetic property calculations. Applying UM methods with TRIC internal coordinates to alkane cracking reactions over H-MFI zeolite showed slight improvements in estimating intrinsic activation entropy, but further refinements are necessary to achieve chemical accuracy.

Keywords: Thermochemistry, Kinetics, Zeolites, Quantum chemical calculations,

Catalysis



CONTENTS



| | |
|---|----|
| Chapter 1 Introduction..... | 1 |
| Chapter 2 Methods | 8 |
| 2.1 Uncoupled Mode Approximation | 8 |
| 2.2 Coordinate Systems | 11 |
| 2.3 Zeolite Modeling..... | 12 |
| 2.4 Computational Details | 15 |
| Chapter 3 Results and Discussions..... | 17 |
| 3.1 Gas Phase Thermodynamic Benchmark | 17 |
| 3.2 Gas Phase Kinetic Benchmark..... | 24 |
| 3.3 Zeolite Reaction Benchmark | 30 |
| Chapter 4 Conclusion | 36 |
| Acknowledgements | 38 |
| Supporting Information | 40 |
| References | 59 |

List of Tables



Table 3.1. Comparative analysis of the computational cost associated with each model

for sampling the PES of 1-propanol. Reprinted with permission from [64].

Copyright 2022, American Chemical Society..... 30

Table 3.2. Adsorption enthalpy (kcal mol^{-1}) at 773K for n-alkane cracking in H-MFI. 34

Table 3.3. Adsorption entropy ($\text{cal mol}^{-1} \text{K}^{-1}$) at 773K for n-alkane cracking in H-MFI.

..... 34

Table 3.4. Intrinsic activation enthalpy (kcal mol^{-1}) at 773K for n-alkane cracking in H-

MFI..... 35

Table 3.5. Intrinsic activation entropy ($\text{cal mol}^{-1} \text{K}^{-1}$) at 773K for n-alkane cracking in

H-MFI..... 35

List of Figures



| | |
|---|----|
| Figure 1.1 Graphical illustration of the uncoupled mode approximation..... | 5 |
| Figure 2.1 Illustration of UM methods (a) sampling of the PES of bending motion of propane (b) sampling of the PES of torsional motion of propane using UM-VT scheme..... | 10 |
| Figure 2.2 QM/MM models for H-MFI. The yellow, red, pink, white, and green colored atoms represent Si, O, Al, H, and Sn atoms, respectively. The spherical atoms are considered QM atoms, whereas the remaining atoms are MM atoms. | 15 |
| Figure 2.3. An example of the sampling of vibrations. | 16 |
| Figure 3.1. Parity analysis of heat capacities. Dashed lines represent the error bars, indicating a range of $\pm 1 \text{ cal mol}^{-1} \text{ K}^{-1}$. Reprinted with permission from [64]. Copyright 2022, American Chemical Society..... | 19 |
| Figure 3.2. Box plot of heat capacities, distinct boxes representing varying numbers of heavy atoms..... | 19 |
| Figure 3.3. Parity analysis of enthalpies $H(298.15 \text{ K})-H(0 \text{ K})$. Dashed lines represent the error bars, indicating a range of $\pm 1 \text{ kcal mol}^{-1}$. Reprinted with permission from [64]. Copyright 2022, American Chemical Society..... | 22 |

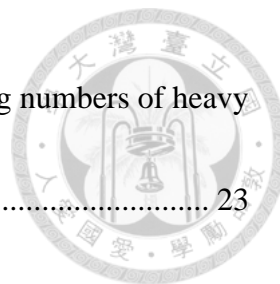


Figure 3.4. Box plot of enthalpies, distinct boxes representing varying numbers of heavy atoms. 23

Figure 3.5. Parity analysis of standard entropies. Dashed lines represent the error bars, indicating a range of $\pm 3.35 \text{ cal mol}^{-1} \text{ K}^{-1}$ ($\pm 1 \text{ kcal mol}^{-1}$ of $T \cdot S$ at 298.15K).

Reprinted with permission from [64]. Copyright 2022, American Chemical Society..... 23

Figure 3.6. Box plot of standard entropies, distinct boxes representing varying numbers of heavy atoms. 23

Figure 3.7. Parity analysis of activation energies of reactions for (a) HIC and (b) TRIC coordinate systems. Dashed lines represent the error bar, indicating a range of $\pm 1 \text{ kcal mol}^{-1}$. Reprinted with permission from [64]. Copyright 2022, American Chemical Society..... 25

Figure 3.8. Parity analysis of pre-exponential factors in logarithm of reactions for (a) HIC and (b) TRIC coordinate systems. Dashed lines represent the error bar, indicating a range of ± 1 in logarithm. Reprinted with permission from [64]. Copyright 2022, American Chemical Society..... 25

Figure 3.9. Diagrammatic representation of reactions involving (a) transition states with four-membered rings (b) transition states with cyclic rings that have more than

four members. Reprinted with permission from [64]. Copyright 2022, American

Chemical Society..... 28

Figure 3.10. Schematic illustration of intrinsic activation enthalpy (ΔH_{int}^\ddagger) and

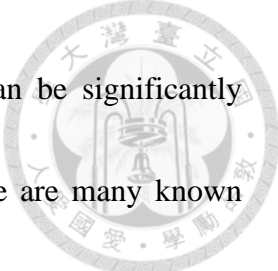
entropy (ΔS_{int}^\ddagger)..... 33



Chapter 1 Introduction



During the 18th century, a distinguished Swedish mineralogist Axel F. Cronstedt discovered a natural mineral that produced vapor when boiled at high temperatures, which he named zeolite.¹ Since then, zeolites have been extensively studied and so far, more than 200 different structures of zeolites have been discovered and synthesized, which are widely used as sorbents and catalysts in industry.^{2,3} Zeolites are crystalline microporous solids composed of tetrahedrally coordinated silicates (SiO_4) with an open structure and innumerable pore channels, which are typically synthesized under hydrothermal conditions. Because of the small-scale pores, zeolites can selectively adsorb molecules and function as a molecular sieve, which has been extensively utilized in gas separation and storage in recent years.^{4,5} The catalytically active sites in zeolites can be created through the substitution of framework silicon (Si) in the zeolite framework by an aluminum (Al) atom and a charge compensating proton (HAlO_4). Due to their excellent hydrothermal and chemical stability, zeolites with Brønsted acid or Lewis acid sites can serve as solid catalysts in various catalytic systems, including biomass conversion⁶⁻⁸, hydrocarbon cracking, and isomerization reactions.⁹⁻¹² In commercial applications, zeolite catalysts are heavily employed by the petroleum industry for fluidized catalytic cracking, representing 95% of the global zeolite consumption.¹³ Experimental studies



have shown that the adsorption and activation of hydrocarbons can be significantly influenced by the zeolite structure and composition.¹⁴⁻¹⁸ Since there are many known zeolite framework structures without applications, it is highly valuable to predict the effect of zeolite framework topology and composition on catalytic activity and selectivity.

Recent advancements in the accuracy and efficiency of quantum chemical methods along with rise in computational capacity have made it possible to employ first-principles theoretical methods for investigating the reaction mechanism and kinetics for various reactions catalyzed by zeolites.¹⁹⁻²¹ Specifically, density functional theory (DFT)^{22, 23} is most widely used for such purpose since it provides a good balance between computational simplicity and accuracy, whereas standard ab initio wave function theories such as MP2 and CCSD(T) scale with the fifth power and worse with the number of electrons. With ab initio calculations, the molecular-scale interactions between zeolite and adsorbate as well as the energetic change of catalytic reactions can be investigated. For comparison with experimental measurements such as equilibrium constants and reaction rates, the calculation of free energy differences, specifically entropies, is required. Unfortunately, calculating entropy contributions to free energies within chemical accuracy²⁴, namely 1 kcal mol⁻¹, is still challenging.²⁵⁻²⁸ Accurately determining energy levels is crucial to obtain thermodynamic or kinetic properties at finite temperatures, but



it can be a challenging task because modeling the full-dimensional potential energy surface (PES) is often computationally impractical, except for extremely small systems.

To address this issue, the usual approach is to treat every vibrational mode as a harmonic oscillator (HO), which allows all frequencies and energy levels to be calculated through a normal mode analysis. However, the HO model has several limitations, especially for low-frequency modes where the potential energy surface often deviates significantly from a quadratic potential. For example, torsions and soft vibrational modes resulting from molecule-surface interactions are particularly difficult to model, making it unsuitable for accurately evaluating reaction rates and free energies of adsorption.²⁹⁻³² To account for anharmonicity, one approach is to scale the calculated harmonic frequencies using an empirical constant known as the scaling factor. However, the accuracy of the results heavily relies on the chosen level of theory, and there is no guarantee that this method will consistently improve the calculated thermodynamic properties.^{33, 34}

In order to accurately capture anharmonicity on the basis of harmonic oscillator, various methods have been proposed. Incorporate with coupled cluster theory (VCC)³⁵⁻³⁷, variational self-consistent field theory (VSCF)³⁸⁻⁴⁰, perturbation theory (VPT)⁴¹⁻⁴³ and configurational interaction (VCI)⁴⁴⁻⁴⁷, quartic force fields (QFFs)⁴⁸ can include higher-order Taylor expansions of PES, which have been shown to produce accurate



experimental vibrational frequencies and rotational constants for small systems. However, these methods are computationally demanding and are therefore limited to small molecules (typically less than 15 atoms).^{49, 50} On the other hand, ab initio molecular dynamics (AIMD) provides an alternative approach to account for anharmonicities in the vibrational spectra since there are no assumptions about the potential energy surface.^{50, 51} By conducting MD simulations directly and Fourier transforming the appropriate time correlation functions (FT-TCF), vibrational spectra and entropy effects can be included.⁵² However, one should note that AIMD is still computationally challenging for larger systems.⁵³ Such problem can be greatly mitigated by if the sum of independent one-dimensional potentials is used to represent the full-dimensional PES. Employing uncoupled mode (UM) approximation, one can obtain energy levels by solving one-dimensional Schrödinger equations with appropriate basis functions. This approach allows the treatment of anharmonicity with a computational cost that scales the same with system size as the standard harmonic oscillator (HO) approach.

However, the UM approximation has one significant drawback since it ignores coupling effects. The accuracy of the UM method depends on how the one-dimensional potentials are defined. The simplest approach to determine the one-dimensional potentials is to sample the PES along each normal mode direction (UM-N), which introduces

artificial coupling between torsional and vibrational motions. This method is not suitable for reproducing torsional potentials accurately.⁵⁴ To overcome this limitation, UM-VT separately samples the PESs along the torsional coordinates and the eigenvectors of the projected Hessian matrix. UM-VT can perform better than UM-N in calculating thermodynamic properties as shown in the previous study.⁵⁴ As for mode coupling, two methods, E-optimized and E'-optimized, can be used to determine the optimal vibrational directions to modulate coupling effects for vibrational frequency calculations.⁵⁵ By employing unitary rotations of the vibrational basis, the E-optimized method aims to minimize the overall squared off-diagonal coupling. On the other hand, the E'-optimized method focuses on minimizing the total squared change in off-diagonal coupling through unitary rotations of the vibrational basis.

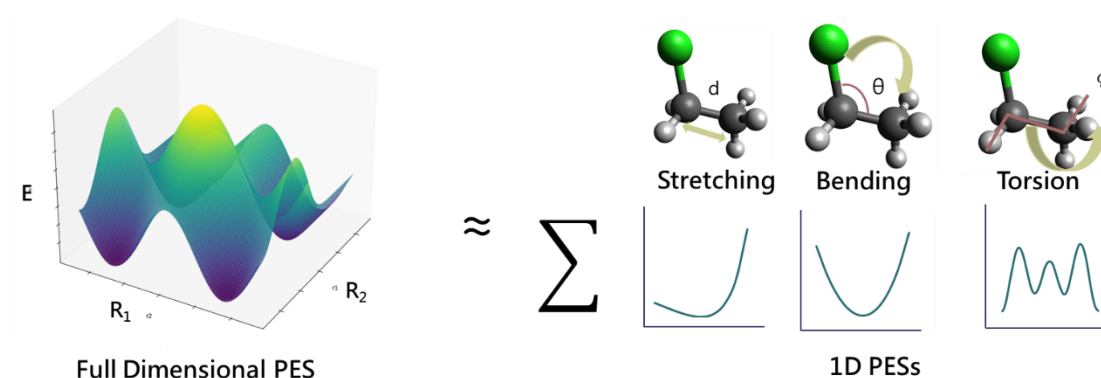


Figure 1.1 Graphical illustration of the uncoupled mode approximation.



In addition to UM approaches that sample along different directions, the selection of coordinate systems can affect the performance of the UM approach as well. Non-linear motion such as bond bending mode and torsional modes are notoriously difficult to address within Cartesian coordinates, where strong artificial coupling between modes would be induced.³² An alternative way is to describe vibrational motion by using redundant internal coordinates (RIC).⁵⁶ However, standard internal coordinate representations may not be appropriate for transition state species containing multiple molecular fragments which cannot be well defined by the bond, bend and dihedral coordinates. Prior research has demonstrated that the incorporation of additional external coordinates can enhance the representation of intermolecular motions in primitive internal coordinate systems. For instance, a novel coordinate system, translation-rotation-internal coordinates (TRIC), introduced translational and rotational coordinates for each molecular fragment.⁵⁷ Another coordinate system proposed method by Billeter and Thiel is the hybrid delocalized internal coordinates (HDLC), which combines primitive internals with Cartesian coordinates of individual atoms.⁵⁸ These hybrid coordinate systems have shown promising results in enhancing geometry optimization convergence. Nevertheless, the utilization of these coordinate systems to enhance the performance of

the UM model in thermodynamic and kinetic calculations has not been extensively explored to date.



In this work, we applied UM methods to both gas phase and zeolitic systems. First, thermodynamic quantities as well as kinetic properties for gas-phase reactions were systematically tested with different UM approaches in various coordinate systems and sampling schemes to evaluate their accuracy. The UM-VT and UM-T methods are found to outperform the other methods in heat capacity, entropy, and pre-exponential factor calculations, while there is no significant difference in enthalpy calculations. Using UM-VT also results in low errors for pre-exponential factors and activation energies, making it a cost-effective method for calculating thermochemistry and kinetic properties for medium- or large-systems. In the second case, we examined the UM approaches within n-alkane cracking reaction in H-MFI. H-MFI zeolite features for its shape selectivity, hydrothermal stability, and anti-coking properties, making it a popular choice for fluid catalytic cracking (FCC), a critical process in the oil refining industry.⁵⁹⁻⁶¹ Besides, substantial theoretical and experimental studies on adsorption and alkane cracking reaction of in zeolites have been made^{10, 12, 59, 60, 62, 63}, which makes it a suitable model system for evaluating UM approaches. The results suggested that UM methods can improve the accuracy of intrinsic activation entropy calculations compared to HO

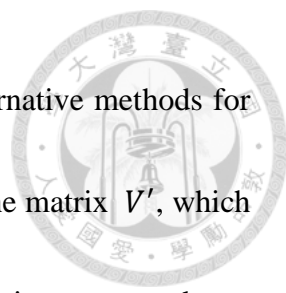
methods; however, further corrections such as multiple-structural approach or relaxed sampling of torsional PES need to be done to comprehensively capture the anharmonicity inside complex reaction systems.



Chapter 2 Methods

2.1 Uncoupled Mode Approximation

The details of UM-N, UM-T and UM-VT can be seen in the previously published work.⁶⁴ UM-N generates one-dimensional potentials for each mode by deforming the geometry in internal coordinates along the direction of the normal mode. A single point calculation is performed for each distorted geometry, and a 1-D PES is interpolated using cubic spline line, as demonstrated in Figure 2.1. In contrast, UM-T and UM-VT project the torsional modes out from the Hessian matrix prior to solving the normal mode problem, to separate them from the vibrational modes. The potentials for torsion are sampled along the torsional coordinate of rotors. UM-T considers other vibrational modes as independent harmonic oscillators, while UM-VT generates potentials for other vibrational modes along the eigenvectors of the projected Hessian matrix.



Apart from UM-N, UM-T, and UM-VT, we also explored alternative methods for constructing potentials that minimize mode-mode coupling. Using the matrix V' , which consists of $3N-6$ eigenvectors derived from the mass-weighted Hessian computed at a stationary point, it is possible to generate an improved set of vibrational coordinates. This involves applying unitary transformations using a vector of angles, θ , to rotate pairs of eigenvectors, resulting in the creation of a new basis, V

$$V = V'U(\theta) \quad (1)$$

where $U(\theta)$ is constructed by combining a series of Jacobi rotations that maintain the orthonormality of V . The value of θ was obtained using two optimization methods, E-optimized and E'-optimized, as proposed by Zimmerman et al.⁵⁵ These approaches begin by computing Hessians at the stationary position and at a grid point for each normal mode, with displacements corresponding to the natural length along each mode. In the case of the E-optimized method, the value of θ is selected to minimize the overall squared off-diagonal coupling in the $3N - 6$ Hessians

$$E = \sum_{m=0}^{3N-6} \sum_{i<j}^{3N-6} (\tilde{H}_{ij}^m)^2 \quad (2)$$

with

$$\tilde{H}_{ij}^m = V^T H^m V \quad (3)$$



where H^m is the m th mass-weighted Hessian, and $m = 0$ denotes the minimum energy geometry. As for E' -optimized, the total squared change in off-diagonal coupling

E' is minimized instead

$$E' = \sum_{m=1}^M \sum_{i<j}^{3N-6} (\tilde{H}_{ij}^m - \tilde{H}_{ij}^0)^2 \quad (4)$$

This strategy aims to minimizing the third derivatives of the energy, while allowing for potentially significant second-order couplings. To break the symmetry, all pairs of eigenvectors were initially rotated by 1 degree before performing the optimization of E and E' . Subsequently, consecutive Jacobi sweeps were carried out over the $M(M - 1)/2$ angles until the minimization was achieved.

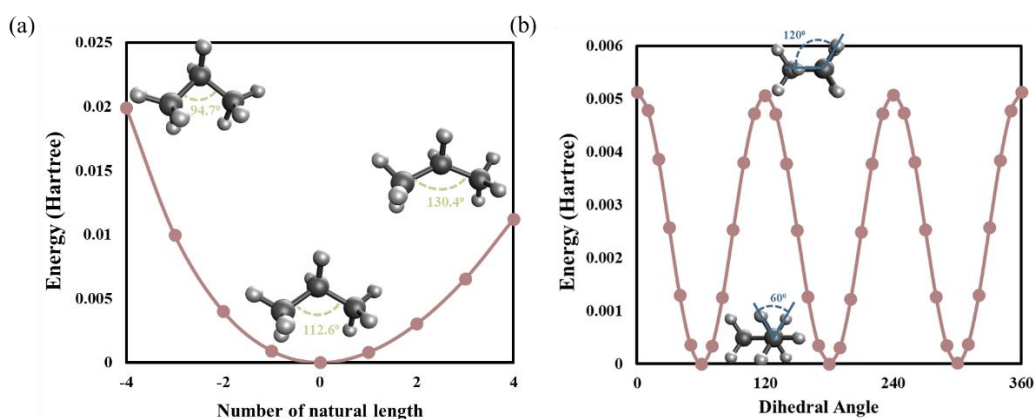


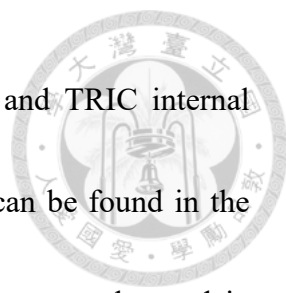
Figure 2.1 Illustration of UM methods (a) sampling of the PES of bending motion of propane (b) sampling of the PES of torsional motion of propane using UM-VT scheme.

2.2 Coordinate Systems



To avoid unrealistic distortions in the geometry of nonlinear modes like bond bends and torsions, it is recommended to sample one-dimensional potential energy surfaces (PES) using internal coordinates instead of Cartesian coordinates.^{32, 65} When sampling the PES in internal coordinates, it is necessary to convert them back to Cartesian coordinates through iterative back-transformation. However, if the chosen internal coordinates are not suitable for the system, the back-transformation may fail to converge, resulting in Cartesian coordinates that do not match the desired internal coordinate values. This issue often arises with transition state species that involve multiple molecular fragments, as the large-amplitude intermolecular motion often result in nearly-linear bend, which makes dihedral angles inadequate to describe such motion. It becomes a serious problem in the case of the uncoupled mode (UM) model, as incorrect steps can lead to deviations between the sampled PES and the actual one, introducing significant errors in energy level and partition function calculations. Therefore, it is essential to choose an appropriate internal coordinate representation that facilitates the transformation between internal and Cartesian coordinate systems for the UM method.

Three internal coordinate systems were investigated in this work, including redundant internal coordinates (RIC), hybrid internal coordinates (HIC), and translation-



rotation-internal coordinates (TRIC). The implementation of HIC and TRIC internal coordinate systems followed previously proposed schemes, which can be found in the published literatures.^{57, 58} RIC employs basic internal coordinates commonly used in geometry optimization, such as bond lengths, bend angles, and dihedral angles. Bonds are identified when the distance between two atoms is less than 1.2 times the sum of their covalent radii, and in the case of molecules with multiple fragments, bonds are established based on the closest distance between each fragment. In HIC, the Cartesian coordinates of each atom are added to the basic internal coordinates to describe collective intramolecular and intermolecular movements. TRIC incorporates three translational and three rotational coordinates as degrees of freedom for each fragment in addition to the internal coordinates, providing a description of the relative position and orientation between these fragments.

2.3 Zeolite Modeling

Cracking of n-alkane on H-MFI zeolite were calculated utilizing quantum mechanics/molecular mechanics (QM/MM) approach, which achieve a trade-off between computational cost and accuracy.^{66, 67} The H-MFI zeolite are modeled by a T437 cluster models, which was terminated with hydrogen atoms by the replacement of terminal oxygen atoms. There exist 12 distinct T-atom positions that can be replaced to generate

an acid site inside MFI, while studies have suggested that the T12 position is preferred⁶⁸,

⁶⁹. The location of the active site at T12 where the straight and sinusoidal channels intersect in MFI is particularly favorable for catalysis because of the ample pore volume surrounding the acid site.

In QM/MM methods, the zeolite cluster models are subdivided into two regions: an active region includes both adsorbate molecules and active sites, while the other region is inactive and comprises zeolite framework atoms that are distant from the active sites, as shown in Figure 2.2. The region where the chemical reaction occurs, i.e., the active site, needs to be accurately calculated using QM methods to accurately describe the formation and breaking of chemical bonds during the chemical reactions. The non-active region of the zeolite framework can be modeled using a molecular mechanics force field, i.e. standard force field of the CHARMM type.⁷⁰⁻⁷², which can account for polarization of the active region and interactions between the adsorbate and the framework through dispersion and electrostatic forces. Using semi-empirical parameters, the MM method reduces the computational cost for simulating environmental effects on reactions. All the geometry optimizations were performed with relaxation of only QM region, whereas the MM atoms were held fixed. Hence, only the interactions between the QM region and MM region will be relevant, which can generally be divided into two parts. The electrostatic

part of the interaction can be described by

$$E_{ES} = \sum_{ij} \frac{q_i q_j}{4\pi\epsilon_0 r_{ij}} \quad (5)$$



where E_{ES} is the electric potential in the QM Hamiltonian due to all the MM atoms; r_{ij} is the distance between particles i and j ; q_j is the partial charge on particle j , which is a force field parameter; ϵ_0 is the dielectric constant. The second component is the interaction energy, which can be described by the Lennard-Jones potential (E_{LJ})

$$E_{LJ} = \sum_{ij} \epsilon_{ij} \left[\left(\frac{R_{ij}}{r_{ij}} \right)^{12} - 2 \left(\frac{R_{ij}}{r_{ij}} \right)^6 \right] \quad (6)$$

where $\epsilon_{ij} = (\epsilon_i \epsilon_j)^{\frac{1}{2}}$, $R_{ij} = (R_i + R_j)/2$, R_i is the van der Waals radius of particle i , and ϵ_i is the characteristic energy of the Lennard-Jones potential of particle i . As shown in the above equations, three parameters are required to describe each type of atom, including charge, van der Waals radius, and characteristic energy. In this work, we utilized the parameter set proposed by Li et al.⁷³

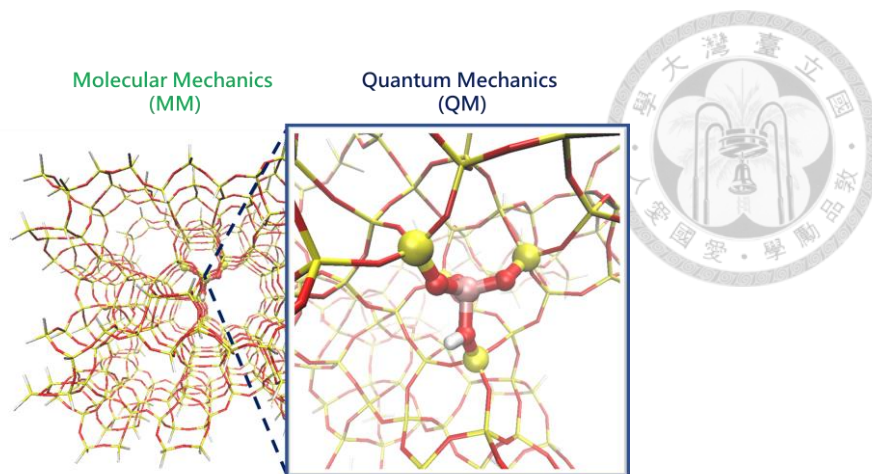


Figure 2.2 QM/MM models for H-MFI. The yellow, red, pink, white, and green colored atoms represent Si, O, Al, H, and Sn atoms, respectively. The spherical atoms are considered QM atoms, whereas the remaining atoms are MM atoms.

2.4 Computational Details

For UM-N and the vibrations of UM-VT, the chosen sampling step size was the corresponding natural length of each vibrational mode. On the other hand, the chosen sampling step size was selected to be $\pi/18$ for the torsions of UM-VT and UM-T. The sampling of vibrations was carried out symmetrically for each mode to the classical turning point or to the point where the energy rose over the cut-off value. As shown in Figure 2.2, the sampling of C=O bond vibration of propanal was terminated at the classical turning point in the negative direction. In contrast, the sampling of torsions was stopped either when the torsion had completed a full rotation (2π) or when the energy exceeded a determined cut-off value. In this study, the cut-off energy selected was 0.05 hartree ($\sim 11,000$ cm⁻¹), which is higher than the classical turning points and torsional

barriers. Previous research has demonstrated that this cut-off energy is sufficient to achieve convergence in the calculation of thermodynamic properties up to 1000 K.⁵⁴

For gas phase molecules, geometry optimization and single point energy calculations were carried out using ω B97X-D functional^{74, 75} and 6-311+G(2df,2dp) basis set. On the other hand, single point energy calculations for QM regions in zeolite models were performed at ω B97X-D/6-311++G(3df,3dp) level of theory. The freezing string method⁷⁶ was employed for the search of transition states, which was subsequently followed by local optimization to refine the guess to the exact transition state. Intrinsic reaction coordinate (IRC) calculations were performed to ensure the connection of each transition state with reactant and product. The calculations mentioned above were performed using a development of the Q-Chem software package.⁷⁷

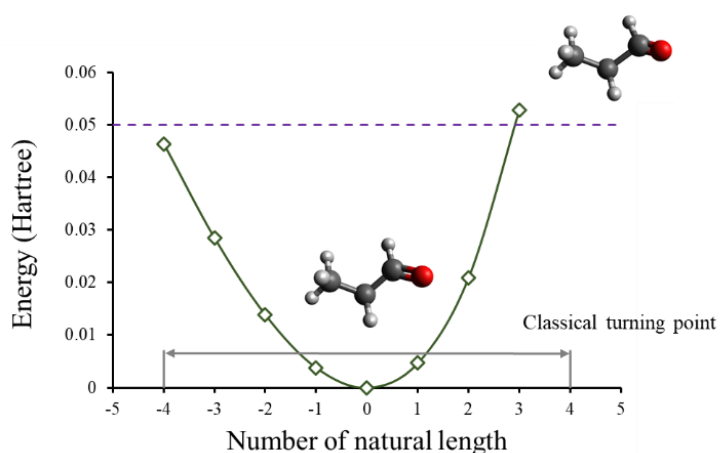


Figure 2.3. An example of the sampling of vibrations.

Chapter 3 Results and Discussions



3.1 Gas Phase Thermodynamic Benchmark

In this section, we evaluated the heat capacities, enthalpies, and entropies of specific molecules calculated by various methods, including UM-N, UM-VT, UM-T, E-optimized, E²-optimized, HO and scaling factor. Scaling factors were obtained from the Computational Chemistry Comparison and Benchmark Database (CCCBDB) and the NIST Chemistry Web book.^{78, 79} The ideal gas heat capacities used as reference values were obtained by extrapolating experimental measurements conducted at different pressures to zero pressure.⁸⁰⁻⁸⁶ Figure 3.1 and Figure 3.2 reveal that although the UM-N method exhibited general improvement compared to the HO approach, it may still have limitations in accurately depicting the periodic potential energy surface related to internal rotations.⁵⁴ Hence, for a more comprehensive treatment of internal rotations and a more accurate representation of the periodic potential, alternative approaches such as UM-T or UM-VT should be considered. UM-T and UM-VT can generally reduce the error to within $1 \text{ cal mol}^{-1} \text{ K}^{-1}$, indicating the separation of internal rotations from other vibrational modes is a crucial aspect of these methods. Furthermore, it is important to highlight that both UM-VT and UM-T methods maintain a consistent level of accuracy even as the

number of heavy atoms increases. On the contrary, employing E-optimized and E'-
optimized approaches for sampling potential energy surfaces yields contrasting outcomes.

Heat capacities calculated using E-optimized exhibit good agreement with experimental values, surpassing that of HO method. However, systematic errors become apparent in the heat capacities derived from E'-optimized, as illustrated in Figure 3.1. The dissimilar performance of E-optimized and E'-optimized can be attributed to their respective optimization objectives. E-optimized strives to minimize overall off-diagonal coupling (as shown in eq (2)), resulting in more precise outcomes. Conversely, E'-optimized prioritizes the reduction of changes in off-diagonal Hessian elements (as shown in eq (4)), placing emphasis on anharmonic couplings. The directions chosen by E'-optimized may inherently introducing harmonic coupling between modes, rendering them unsuitable for constructing the one-dimensional potentials utilized in UM calculations. As a result, employing E'-optimized directions can yield improper representations of the potential energy surface (PES) and lead to large errors in thermodynamic property calculations. Additionally, our findings indicate that the use of scaling factors can yield accurate results in the calculations of heat capacities, effectively matching them with the experimental data.

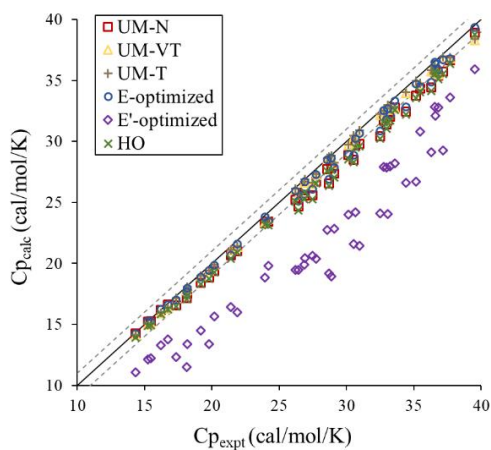


Figure 3.1. Parity analysis of heat capacities. Dashed lines represent the error bars, indicating a range of $\pm 1 \text{ cal mol}^{-1} \text{ K}^{-1}$. Reprinted with permission from [64]. Copyright

2022, American Chemical Society.

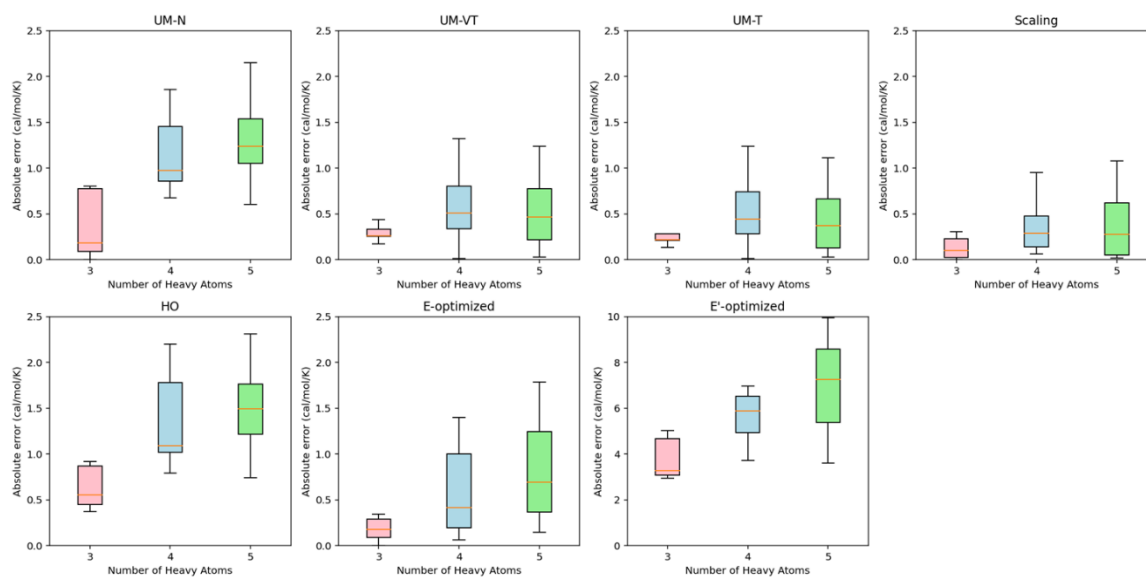


Figure 3.2. Box plot of heat capacities, distinct boxes representing varying numbers of

heavy atoms.



Aside from evaluating heat capacities, we examined the performance of various UM methods for calculating enthalpies and entropies as well. To gather the scarce reference data for enthalpies and entropies, we collected information from NIST⁸⁷. These reference values are primarily obtained from spectroscopic data using statistical mechanics, incorporating internal corrections but disregarding anharmonicity or coupling effects.⁸⁸⁻

⁹⁰ In enthalpy calculations, E'-optimized still give large error owing to an inappropriate treatment for mode coupling. The other methods generally produce results fall within a ± 1 kcal/mol error range, as depicted in Figure 3.3 and Figure 3.4. However, the accuracy of entropy calculations varies significantly across the different methods, as depicted in Figure 3.5 and Figure 3.6. UM-VT and UM-T demonstrate the highest level of accuracy, followed by scaling, E-optimized, UM-N, HO, and E'-optimized. Align with the findings in heat capacity calculations, the HO model underestimates entropies owing to its limited handling of internal rotors. E-optimized does not show considerable improvement compared to UM-N and HO. On the other hand, the RMS error of E'-optimized ($12.71 \text{ cal mol}^{-1} \text{ K}^{-1}$) is nearly four times higher than that of the HO model ($3.71 \text{ cal mol}^{-1} \text{ K}^{-1}$).

In contrast to the previous results in heat capacity calculations, the use of the scaling factor leads to a larger error bar when predicting standard entropies of larger molecules.

The enthalpy is not method-sensitive since it is based on the following equation

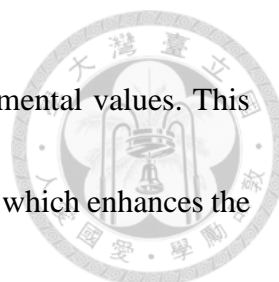
$$H = RT^2 \frac{\partial \ln(Q)}{\partial T} + RT \quad (7)$$

Not only the logarithm function diminishes the differences of the calculated partition function, but the first derivative of logarithm of partition function with respect to temperature cancel out errors. Therefore, even the simplest HO model can give quite accurate results for enthalpy calculations. On the other hand, entropy is closely related to the logarithm of the partition function

$$S = RT \frac{\partial \ln(Q)}{\partial T} + R \ln(Q) \quad (8)$$

The entropy calculations are therefore greatly affected by the choice of methods. Also, the heat capacity is calculated by the derivative of enthalpy with respect to temperature (second derivative of partition function), which makes it more sensitive to the accuracy of calculated partition function.

While UM-T and UM-VT show good agreement with reference values for thermodynamic properties, it does not necessarily mean that the fundamental frequencies calculated by these methods are more accurate than the HO model, as shown in Table S4 to S13. Previous studies have indicated that low-frequency modes often possess a delocalized nature, with vibrational motions occurring throughout the entire molecule.⁹¹ As a result, attempting to localize torsional modes to individual dihedral coordinates would inevitably lead to inaccuracies. On the contrary, the E-optimized model produces



vibrational frequencies that exhibit excellent agreement with experimental values. This can be attributed to the optimization of overall off-diagonal coupling, which enhances the accuracy of vibrational structure calculations. These findings are in line with the previous results reported in the literature.⁵⁵

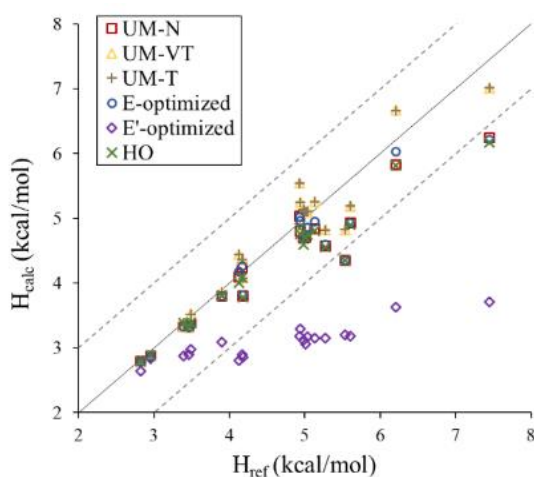


Figure 3.3. Parity analysis of enthalpies $H(298.15\text{ K})-H(0\text{ K})$. Dashed lines represent the error bars, indicating a range of $\pm 1\text{ kcal mol}^{-1}$. Reprinted with permission from [64].

Copyright 2022, American Chemical Society.

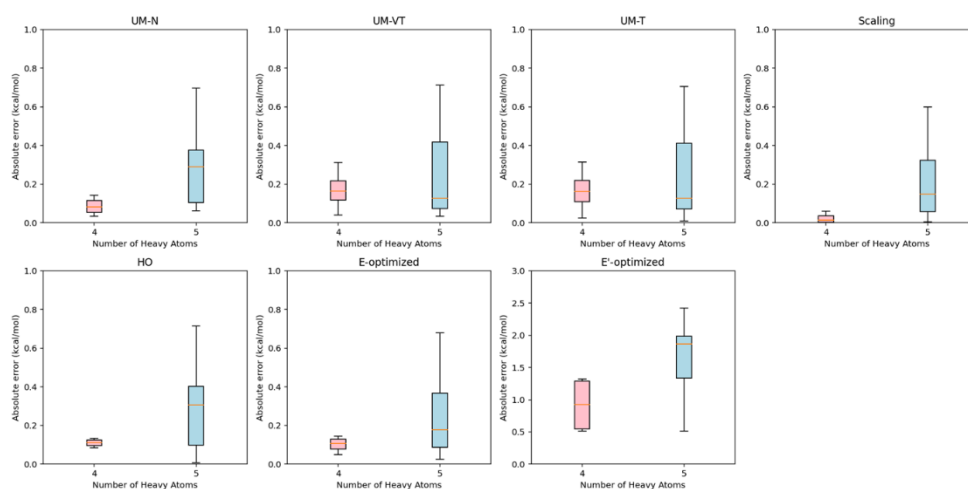




Figure 3.4. Box plot of enthalpies, distinct boxes representing varying numbers of heavy atoms.

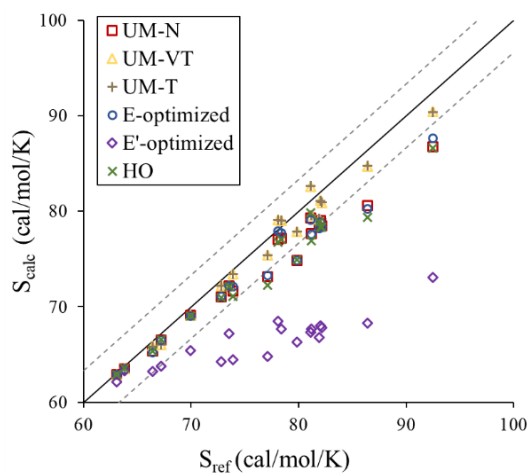


Figure 3.5. Parity analysis of standard entropies. Dashed lines represent the error bars, indicating a range of $\pm 3.35 \text{ cal mol}^{-1} \text{ K}^{-1}$ ($\pm 1 \text{ kcal mol}^{-1}$ of $T \cdot S$ at 298.15K). Reprinted with permission from [64]. Copyright 2022, American Chemical Society.

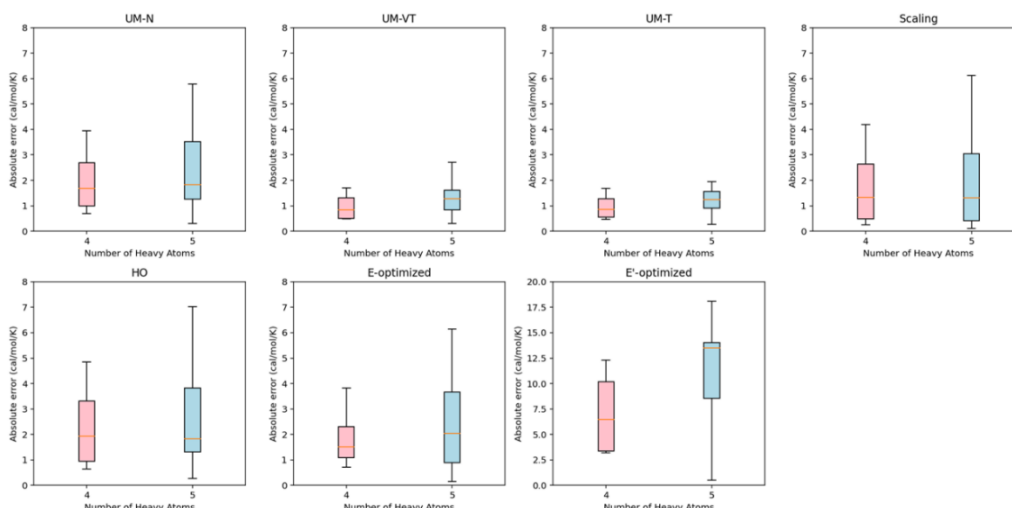
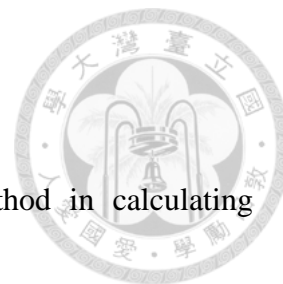


Figure 3.6. Box plot of standard entropies, distinct boxes representing varying numbers of heavy atoms.

3.2 Gas Phase Kinetic Benchmark



After carefully examining the accuracy of each UM method in calculating thermodynamic properties, we also assessed the accuracy of these methods in calculating kinetic parameters. Here, we compared the experimental activation energy and Arrhenius pre-exponential values of nineteen unimolecular gas-phase reactions⁹²⁻¹⁰³ with the results derived from various UM methods in combination of different coordinate systems (RIC, HIC, and TRIC). The complete list of reactions, along with the corresponding reaction temperatures, is presented in Table S1. Our results, as shown in Table S2 and Table S3, indicated that approximately half of the reactions could not be properly calculated using RIC due to the inadequate characterization of large-amplitude interfragmentary motion by bond, bend, and dihedral angles.

On the contrary, the HIC and TRIC internal coordinate systems addressed this issue by incorporating augmented Cartesian coordinates or translation-rotation coordinates into the internal coordinates. Analyzing Figure 3.7, we found that while the activation energies calculated in TRIC were slightly more accurate than those calculated in HIC, the RMS errors for both methods fell within the range of 1-2 kcal/mol. This suggests that the choice of the model does not significantly impact the accuracy of the activation energy, which aligns with our observations in the enthalpy calculations.

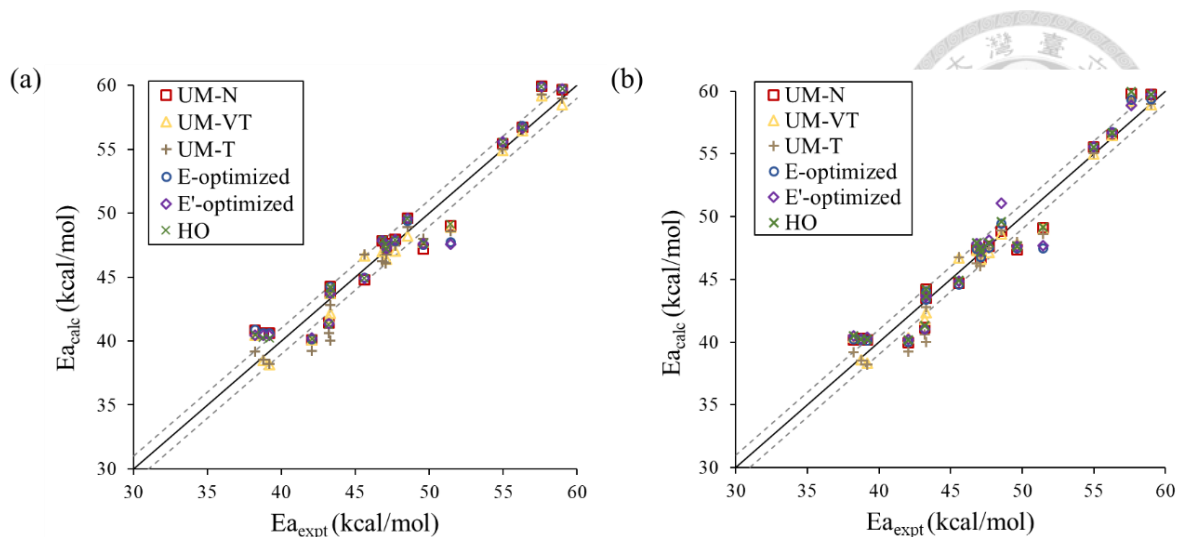


Figure 3.7. Parity analysis of activation energies of reactions for (a) HIC and (b) TRIC coordinate systems. Dashed lines represent the error bar, indicating a range of ± 1 kcal mol^{-1} . Reprinted with permission from [64]. Copyright 2022, American Chemical Society.

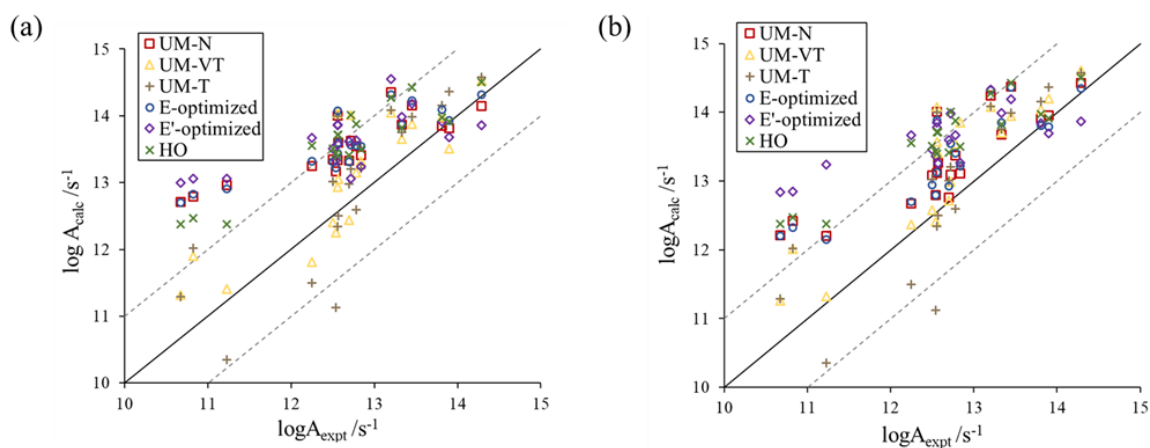
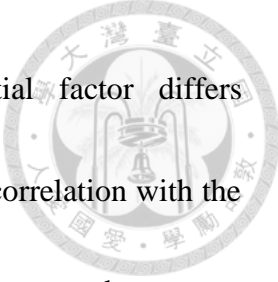


Figure 3.8. Parity analysis of pre-exponential factors in logarithm of reactions for (a) HIC and (b) TRIC coordinate systems. Dashed lines represent the error bar, indicating a range of ± 1 in logarithm. Reprinted with permission from [64]. Copyright 2022,

American Chemical Society.



The precision of the calculated Arrhenius pre-exponential factor differs significantly across the various methods, primarily due to its strong correlation with the activation entropy, which is in close relation with the entropy change between the reactant and transition state species. To accommodate the wide range of magnitudes observed for different reactions, the logarithmic values of the pre-exponential factor ($\log A/s^{-1}$) are presented in Figure 3.8. The majority of $\log A$ values obtained through the UM-VT and UM-T methods fall within the ± 1 error range, as shown in Figure 3.8, suggesting that the inclusion of additional rotor treatment indeed enhances accuracy. Conversely, the remaining methods exhibit a tendency to overestimate the $\log A$ values. Notably, the E'-optimized method demonstrates the highest RMS errors, as previously discussed. This discrepancy can be attributed to the selection of directions by E'-optimized, which primarily prioritize minimizing anharmonic couplings. Unfortunately, this approach introduces strong harmonic coupling between modes, ultimately hindering the improvement of UM calculations' accuracy. It is important to highlight that the UM-VT method slightly outperforms the UM-T method in predicting kinetic properties, potentially due to its superior representation of anharmonic motions in transition state species. When assessing $\log A$ values, the RMS errors for UM-VT using HIC and TRIC coordinate systems are 0.64 and 0.68, respectively, indicating comparable performance



between the two coordinate systems. However, for the other sampling schemes, the TRIC coordinate system generally yields slightly lower RMS errors compared to HIC. This suggests that segregating the degrees of freedom for intramolecular and intermolecular motions could describe transition state species more properly. In addition to the UM methods, we also evaluated the performance of scaling factor on the calculation of the activation energies and pre-exponential factors. It was found that the scaling factor cannot make any difference on the accuracy of calculated kinetic parameters, which was resulted from the same scaling of partition function of both reactant and transition state.

It is important to highlight that despite its limitations, the HO model can successfully predict the Arrhenius pre-exponential factor for certain reactions. Specifically, reactions involving four-membered transition states, like the dehydrohalogenation of alkyl halides (Figure 3.9a), exhibit accurate predictions regardless of the model used, including the HO approach. However, for reactions involving cyclic transition states with rings comprising more than four members, such as ester pyrolysis (Figure 3.9b), a more precise treatment of rotational entropy is necessary to correctly estimate the Arrhenius pre-exponential factor. This is due to the fixation of multiple rotors during the formation of the transition states. Therefore, the significance of considering anharmonic effects in improving predictions depends on the structural

characteristics of the transition state species. As a result, the extent of improvement may not be uniformly pronounced across all examined reactions.

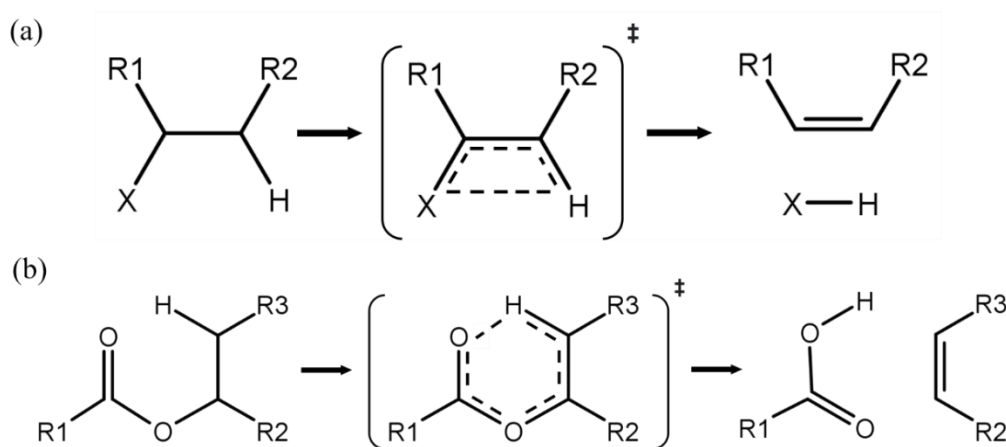
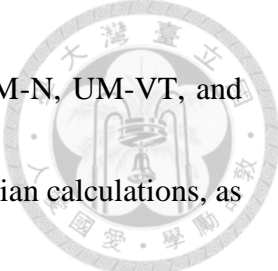


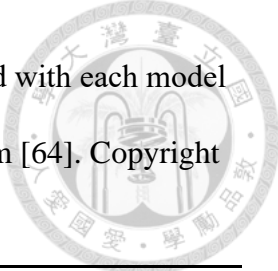
Figure 3.9. Diagrammatic representation of reactions involving (a) transition states with four-membered rings (b) transition states with cyclic rings that have more than four members. Reprinted with permission from [64]. Copyright 2022, American Chemical Society.

Furthermore, we conducted a comparison of the CPU time associated with each method to assess their computational cost. All five UM methods (UM-N, UM-VT, UM-T, E-optimized, and E'-optimized) necessitate the Hessian matrix at the local minimum geometry, as stated in the methodology section. However, the E-optimized and E'-optimized models require additional $3N-6$ Hessians near the local minimum geometry to obtain optimal sampling directions. Consequently, the computational costs of E-



optimized and E'-optimized are unavoidably higher compared to UM-N, UM-VT, and UM-T. Table 3.1 displays the number of single point energy and Hessian calculations, as well as the CPU time required to sample the PES of 1-propanol. The CPU time exhibits the following trend: E'-optimized \approx E-optimized > UM-VT > UM-N > UM-T > HO = Scaling. The CPU time for E-optimized (80935 s) and E'-optimized (81961 s) is three to four times higher than that of UM-N (18083 s) and UM-VT (24138 s), and ten times higher than that of UM-T (7822 s). It is important to note that this ratio is expected to increase with larger system sizes since E-optimized or E'-optimized necessitates one Hessian calculation per normal mode. To strike a balance between accuracy and computational costs, it is recommended to employ the UM-T model for calculating molecular thermochemistry in the medium- or low-temperature range, where the impact of anharmonicity in vibrations is negligible. For scenarios where the influence of anharmonic vibrations may be significant, such as calculating partition functions of transition state species, particularly for reactions occurring in complex environments, the UM-VT method is recommended.^{26, 31}

Table 3.1. Comparative analysis of the computational cost associated with each model for sampling the PES of 1-propanol. Reprinted with permission from [64]. Copyright 2022, American Chemical Society.



| | UM-N | UM-VT | UM-T | E-optimized | E'-optimized | HO | Scaling |
|---------------------------|-------|-------|------|-------------|--------------|------|---------|
| No. Single points | 256 | 342 | 72 | 259 | 260 | 0 | 0 |
| No. Hessians | 1 | 1 | 1 | 31 | 31 | 1 | 1 |
| CPU time (s) ^a | 18083 | 24138 | 6415 | 80935 | 81961 | 2006 | 2006 |

^aAll timings were performed using the Q-Chem software package on a single core of a 2.0 GHz AMD EPYC Rome 64-core processor machine.

3.3 Zeolite Reaction Benchmark

In this section, we conducted a comparison of experimental adsorption enthalpies/entropies and intrinsic activation enthalpies/entropies of alkane cracking over H-MFI with those obtained through different calculation methods. The methods included uncoupled mode (UM) methods, scaling factor, and quasi-RRHO¹⁰⁴, all within the quantum mechanics/molecular mechanics (QM/MM) model. We calculated the thermodynamic properties using these approaches (773K) and compared the results to Configurational-Bias Monte Carlo simulations (CBMC)²¹ (773K) and experimental data (300-400K)^{62, 105}. We did not examine the performance of E-optimized and E'-optimized approaches due to the high computational demands of calculating additional Hessians in zeolitic systems. Also, considering that the TRIC coordinate system generally produces

better results in gas-phase reaction calculations, we performed the UM methods using TRIC coordinate systems for the calculation of intrinsic activation parameters. The intrinsic activation parameters are defined as the difference of the properties between transition states and adsorbed states, as illustrated in Figure 3.10. Since there are different bond i for the activation of butane cracking, we employed Boltzmann weighted average to obtain results that can be compared with experimental or Monte Carlo simulation data.²¹ The Boltzmann average were calculated based on the following equation^{21, 106}

$$\Delta H_{int}^{\ddagger} = \frac{\sum_i \Delta H_{int,i}^{\ddagger} \exp\left(-\frac{\Delta A_{int,i}^{\ddagger}}{RT}\right)}{\sum_i \exp\left(-\frac{\Delta A_{int,i}^{\ddagger}}{RT}\right)} = \Delta U_{int}^{\ddagger} - RT \quad (9)$$

$$\Delta A_{int}^{\ddagger} = \frac{\sum_i \Delta A_{int,i}^{\ddagger} \exp\left(-\frac{\Delta A_{int,i}^{\ddagger}}{RT}\right)}{\sum_i \exp\left(-\frac{\Delta A_{int,i}^{\ddagger}}{RT}\right)} \quad (10)$$

$$\Delta S_{int}^{\ddagger} = \frac{\Delta U_{int}^{\ddagger} - \Delta A_{int}^{\ddagger}}{T} \quad (11)$$

The calculated adsorption thermodynamics at 773K were listed in Table 3.2 and Table 3.3. The results demonstrate that the adsorption enthalpies remain relatively consistent across different methods. However, the accuracy of the adsorption entropies varies with the choice of models. The uncoupled mode (UM) methods generally offer more accurate results compared to the HO or quasi-RRHO models. Despite this improvement, there is still a discrepancy between the calculated values and the reference data. Scaling factor, on the other hand, can also improve the accuracy based on the harmonic approximation.



Calculated intrinsic activation enthalpy and entropy for cracking at T12 site at 773K were listed in Table 3.4 and Table 3.5. Similar to the observations in adsorption thermodynamics, the choice of model does not greatly affect the accuracy of intrinsic activation enthalpies ($\Delta H_{int}^{\ddagger}$). The errors of both UM and HO methods falls within the range of 2 kcal/mol. However, the accuracy of calculated intrinsic activation entropies ($\Delta S_{int}^{\ddagger}$) are more sensitive to the choice of model. Considering local anharmonicity, the uncoupled mode (UM) methods generally outperformed the harmonic oscillator (HO) methods in calculations related to intrinsic activation entropy. Although the results obtained through the UM method show improvement compared to the HO method, there is still a small difference between the calculated $\Delta S_{int}^{\ddagger}$ and experimental $\Delta S_{int}^{\ddagger}$. Notably, the UM-T method showed less accurate results compared to HO results, which may be attributed to an inappropriate description of torsional motions of alkane within zeolite systems. The first challenge arises from the fact that multiple conformations of molecules collectively contribute to the entropy and free energy. Especially, torsions in catalytic system are usually unsymmetrical, the local minima sampled along the torsional coordinates are distinguishable. In other words, a single optimized conformation derived from a normal mode analysis is inadequate to capture the full conformational landscape and accurately estimate these thermodynamic quantities.³⁰ Such issues can be treated by

summing the torsional contributions from a list of distinguishable conformers, which has been shown to improve the accuracy of entropy calculations in complex molecular systems previously^{30, 107} Additionally, if the initial geometry of the adsorbate is positioned too close to the zeolite framework, the sampling of torsional modes may terminate prematurely upon reaching the energy cut-off. To address this issue, we can enhance the sampling process of torsional potential energy surfaces (PES) by freezing the dihedral angle and optimizing the geometry.¹⁰⁸ The incorporation of relaxed torsional PES for each internal rotor has the potential to enhance the accuracy of computed energy levels and entropy values.

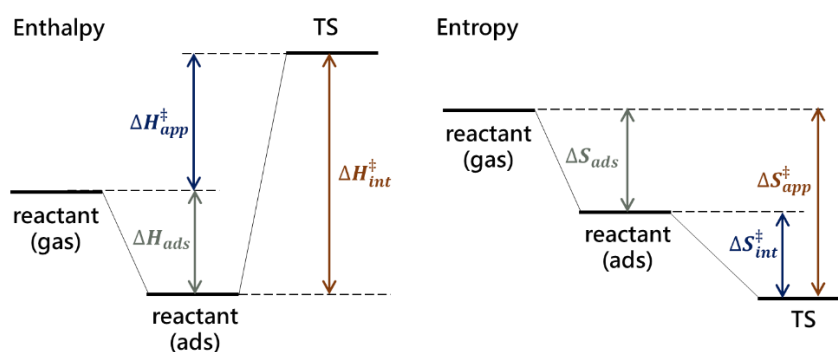


Figure 3.10. Schematic illustration of intrinsic activation enthalpy ($\Delta H_{int}^{\ddagger}$) and entropy

($\Delta S_{int}^{\ddagger}$).

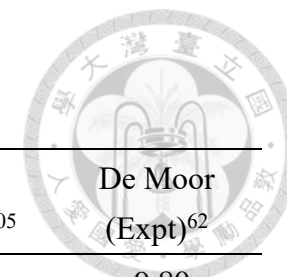


Table 3.2. Adsorption enthalpy (kcal mol⁻¹) at 773K for n-alkane cracking in H-MFI.

| ΔH_{ads}^\ddagger | UM-N | UM-VT | UM-T | HO | quasi-RRHO | Scaling | Janda (CBMC) ²¹ | Eder (Expt) ¹⁰⁵ | De Moor (Expt) ⁶² |
|---------------------------|--------|--------|--------|--------|------------|---------|-------------------------------|-------------------------------|---------------------------------|
| propane | -14.34 | -14.10 | -11.23 | -11.47 | -13.62 | -11.59 | -10.52 | -10.76 | -9.80 |
| butane | -15.30 | -13.38 | -13.15 | -13.86 | -15.54 | -12.67 | -12.91 | -13.86 | -12.43 |

Table 3.3. Adsorption entropy (cal mol⁻¹ K⁻¹) at 773K for n-alkane cracking in H-MFI.

| ΔS_{ads}^\ddagger | UM-N | UM-VT | UM-T | HO | quasi-RRHO | Scaling | Janda (CBMC) ²¹ | Eder (Expt) ¹⁰⁵ | De Moor (Expt) ⁶² |
|---------------------------|--------|--------|--------|--------|------------|---------|-------------------------------|-------------------------------|---------------------------------|
| propane | -35.37 | -35.61 | -38.00 | -38.72 | -37.76 | -36.81 | -23.90 | -24.38 | -22.47 |
| butane | -32.50 | -36.33 | -31.55 | -34.42 | -33.70 | -32.03 | -26.05 | -28.44 | -24.86 |

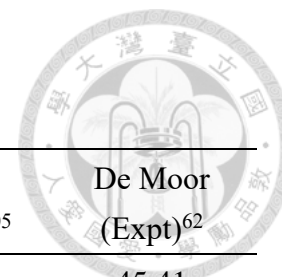


Table 3.4. Intrinsic activation enthalpy (kcal mol⁻¹) at 773K for n-alkane cracking in H-MFI.

| $\Delta H_{int}^{\ddagger}$ | UM-N | UM-VT | UM-T | HO | quasi-RRHO | Scaling | Janda (CBMC) ²¹ | Eder (Expt) ¹⁰⁵ | De Moor (Expt) ⁶² |
|-----------------------------|-------|-------|-------|-------|------------|---------|-------------------------------|-------------------------------|---------------------------------|
| propane | 43.98 | 44.60 | 44.49 | 44.00 | 44.43 | 44.22 | 45.89 | 46.37 | 45.41 |
| butane | 41.71 | 41.21 | 40.84 | 41.47 | 42.84 | 41.58 | 43.50 | 44.69 | 43.26 |

Table 3.5. Intrinsic activation entropy (cal mol⁻¹ K⁻¹) at 773K for n-alkane cracking in H-MFI.

| $\Delta S_{int}^{\ddagger}$ | UM-N | UM-VT | UM-T | HO | quasi-RRHO | Scaling | Janda (CBMC) ²¹ | Eder (Expt) ¹⁰⁵ | De Moor (Expt) ⁶² |
|-----------------------------|-------|--------|--------|--------|------------|---------|-------------------------------|-------------------------------|---------------------------------|
| propane | -3.10 | -1.88 | -0.54 | -0.88 | 0.57 | -1.22 | -5.02 | -5.26 | -7.17 |
| butane | -9.45 | -10.07 | -12.55 | -11.64 | -11.94 | -11.89 | -5.98 | -4.54 | -8.13 |



Chapter 4 Conclusion

In order to improve the accuracy of thermochemical and kinetic predictions, we utilized UM methods that consider the sum of independent one-dimensional (1D) anharmonic potential energy surface as representation of full-dimensional potential energy surface. To approach the highest possible accuracy within the UM model, we first employed five different potential energy surface (PES) sampling schemes, namely UM-N, UM-VT, UM-T, E-optimized, and E'-optimized, and extensively benchmarked these methods on molecular thermochemistry (heat capacities, enthalpies, and entropies) and kinetic properties (activation energies and pre-exponential factors) of selected reactions.

In the UM-N method, 1D potentials are constructed by sampling along the direction of each normal mode. By accounting for local anharmonicities, UM-N yields slightly improved accuracy compared to the HO model. UM-VT and UM-T involve sampling the potentials of internal rotations to accurately capture their anharmonic behavior. Additionally, UM-VT samples the vibrational modes to capture more system anharmonicity, while UM-T treats other vibrational modes as harmonic oscillators. Both UM-VT and UM-T exhibit good performance in predicting thermodynamic properties, with UM-VT demonstrating slightly higher accuracy for kinetic property calculations.



For E-optimized and E'-optimized, potentials are constructed along specific directions that minimize off-diagonal coupling and change in off-diagonal coupling, respectively, over a grid of Hessian matrices. E-optimized generally outperforms the HO model in terms of accuracy. However, E'-optimized can introduce systematic errors due to its focus on reducing changes in off-diagonal Hessian elements, which only represent anharmonic couplings. Consequently, the directions determined by E'-optimized may lead to strong harmonic coupling between modes, making them unsuitable for constructing potentials in uncoupled mode calculations. Apart from investigating various sampling methods, we also evaluated the impact of frequency scaling factors. Our findings indicate that scaling factors can yield accurate results for properties that are not significantly affected by partition function accuracy. However, when considering properties such as entropies, the uncoupled mode (UM) methods, specifically UM-VT and UM-T, prove to be more suitable options.

In addition to exploring various sampling methods, we also investigated the impact of internal coordinate systems on the performance of molecular reactions in the gas phase. Internal coordinate systems play a crucial role in accurately describing the geometry and motion of molecules during reactions, where the straightforward redundant internal coordinates (RIC) fail to accurately characterize large-amplitude interfragmentary motion

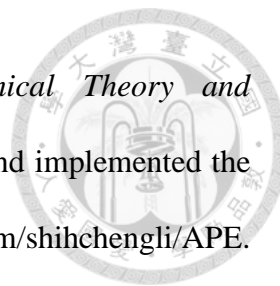


in a transition state. To mitigate this problem, hybrid internal coordinate (HIC) or translation-rotation-internal coordinate (TRIC) systems can be employed. The results indicate that the TRIC system slightly outperforms the HIC system in calculating kinetic parameters especially for Arrhenius pre-exponential factors, suggesting that intra- and intermolecular motions should be describe separately to improve the performance of the UM model for kinetic property calculations. Furthermore, we investigated the UM methods incorporating with TRIC internal coordinates on the performance of alkane cracking reactions over H-MFI zeolite. The results suggested that though UM methods can slightly improve the accuracy of estimated intrinsic activation entropy, further improvements need to be made to achieve chemical accuracy. We suggested that by summing torsional contributions from distinguishable conformers, the accuracy of entropy calculations in complex molecular systems can be improved. Furthermore, enhancing the sampling process of torsional potential energy surfaces by freezing the dihedral angle and optimizing the geometry addresses issues arising from adsorbate positioning, leading to more accurate energy levels and entropy values.

Acknowledgements

This work was collaborated with Shih-Cheng Li and has been published as Li, S.-C.; Lin, Y.-C.; Li, Y.-P., Comparative Analysis of Uncoupled Mode Approximations for

Molecular Thermochemistry and Kinetics. *Journal of Chemical Theory and Computation* **2022**, 18 (11), 6866-6877. Shih-Cheng Li developed and implemented the methods into python code, which is available at <https://github.com/shihchengli/APE>. Yen-Chun Lin collected the experimental data, performed calculations of UM methods as well as data analysis, and evaluated the computational costs of each method.



Supporting Information



Table S1. Test reactions selected in this work.

| Rxn | | T range (K) |
|-----|--|---------------|
| 1 | $\text{ClCH}_2\text{C}(\text{O})\text{OC}_2\text{H}_5 \rightarrow \text{C}_2\text{H}_4 + \text{CH}_2\text{ClC}(\text{O})\text{OH}$ | 633.45-665.05 |
| 2 | $\text{C}_2\text{H}_5\text{C}(\text{O})\text{OC}_2\text{H}_5 \rightarrow \text{C}_2\text{H}_5\text{COOH} + \text{C}_2\text{H}_4$ | 913-1100 |
| 3 | $\text{ClCH}_2\text{CH}_2\text{C}(\text{O})\text{OC}_2\text{H}_5 \rightarrow \text{C}_2\text{H}_4 + \text{ClCH}_2\text{CH}_2\text{C}(\text{O})\text{OH}$ | 633.45-665.05 |
| 4 | $\text{CHCl}_2\text{C}(\text{O})\text{OCH}(\text{CH}_3)_2 \rightarrow \text{CHCl}_2\text{C}(\text{O})\text{OH} + \text{CH}_3\text{CH}=\text{CH}_2$ | 566-599 |
| 5 | $\text{ClCH}_2\text{CH}_2\text{C}(\text{O})\text{OCH}(\text{CH}_3)_2 \rightarrow \text{CH}_2\text{ClCH}_2\text{C}(\text{O})\text{OH} + \text{CH}_3\text{CH}=\text{CH}_2$ | 576.15-624.95 |
| 6 | $\text{BrCH}_2\text{C}(\text{O})\text{OCH}(\text{CH}_3)_2 \rightarrow \text{CH}_2\text{BrC}(\text{O})\text{OH} + \text{CH}_3\text{CH}=\text{CH}_2$ | 563.65-623.25 |
| 7 | $\text{CH}_2\text{OHC}(\text{O})\text{OCH}(\text{CH}_3)_2 \rightarrow \text{CH}_2\text{OHC}(\text{O})\text{OH} + \text{CH}_3\text{CH}=\text{CH}_2$ | 573.35-623.25 |
| 8 | $\text{CH}_3\text{C}(\text{O})\text{OC}_2\text{H}_5 \rightarrow \text{CH}_3\text{C}(\text{O})\text{OH} + \text{C}_2\text{H}_4$ | 650.45-700.35 |
| 9 | $\text{CH}_2=\text{CHCH}_2\text{CH}_2\text{OH} \rightarrow \text{CH}_2\text{O} + \text{CH}_3\text{CH}=\text{CH}_2$ | 636-714 |
| 10 | $\text{CH}_2=\text{CHCH}_2\text{C}(\text{O})\text{OC}_2\text{H}_5 \rightarrow \text{C}_2\text{H}_4 + \text{CH}_2=\text{CHCH}_2\text{C}(\text{O})\text{OH}$ | 633-693 |
| 11 | $\text{CH}_3\text{SCH}_2\text{CH}=\text{CH}_2 \rightarrow \text{CH}_3\text{CH}=\text{CH}_2 + \text{CH}_2=\text{S}$ | 649.15-691.15 |
| 12 | $\text{CH}_2=\text{CHCH}_2\text{CH}_2(\text{CH}_3)\text{OH} \rightarrow \text{CH}_3\text{CH}_2=\text{O} + \text{CH}_3\text{CH}=\text{CH}_2$ | 635.7-713.7 |
| 13 | $\text{CH}_2\text{ClCH}_2\text{CN} \rightarrow \text{CH}_2\text{CHCN} + \text{HCl}$ | 942-1150 |
| 14 | $(\text{CH}_3)_2\text{CClCH}_2\text{Cl} \rightarrow \text{CH}_2=\text{C}(\text{CH}_3)\text{CH}_2\text{Cl} + \text{HCl}$ | 613-693 |
| 15 | $\text{n-C}_3\text{H}_7\text{Cl} \rightarrow \text{CH}_3\text{CH}=\text{CH}_2 + \text{HCl}$ | 672-734 |
| 16 | $\text{C}_2\text{H}_5\text{Cl} \rightarrow \text{HCl} + \text{C}_2\text{H}_4$ | 663.15-683.15 |
| 17 | $\text{tert-C}_4\text{H}_9\text{OCH}_3 \rightarrow \text{CH}_3\text{OH} + \text{iso-C}_4\text{H}_8$ | 623-763 |
| 18 | $(\text{CH}_3)_2\text{CClC}(\text{O})\text{OCH}_3 \rightarrow \text{CH}_2=\text{C}(\text{CH}_3)\text{C}(\text{O})\text{OCH}_3 + \text{HCl}$ | 633-693 |
| 19 | $(\text{CH}_3)_2\text{CClC}(\text{O})\text{CH}_3 \rightarrow \text{CH}_2=\text{C}(\text{CH}_3)\text{C}(\text{O})\text{CH}_3 + \text{HCl}$ | 612.95-667.65 |



Table S2. Activation energies of selected gas-phase reactions calculated with RIC (kcal/mol). Missing values are caused by the failure in the back-transformation from internal to Cartesian coordinates.

| Rxn | Expt | RIC | | | |
|-----|--------------------|-------|-------|-------------|--------------|
| | | UM-N | UM-VT | E-Optimized | E'-Optimized |
| 1 | 47.08 ^a | - | - | 47.14 | 45.19 |
| 2 | 48.52 ^b | - | - | - | - |
| 3 | 47.04 ^a | - | - | - | 47.8 |
| 4 | 42.07 ^c | - | - | - | 40.97 |
| 5 | 43.21 ^c | - | - | - | 41.41 |
| 6 | 43.30 ^d | - | - | - | 43.29 |
| 7 | 43.30 ^c | - | - | - | - |
| 8 | 47.70 ^e | 47.76 | 47.39 | - | - |
| 9 | 39.20 ^f | 40.09 | 38.20 | 40.21 | 40.36 |
| 10 | 46.84 ^g | 47.89 | 47.56 | 47.85 | 49.3 |
| 11 | 38.24 ^h | 40.26 | 40.46 | - | 40.87 |
| 12 | 38.77 ^f | 40.28 | 38.61 | - | 40.38 |
| 13 | 57.60 ⁱ | - | - | - | 59.72 |
| 14 | 49.62 ^j | 47.35 | 47.80 | 47.39 | 47.63 |
| 15 | 54.97 ^k | 55.62 | 55.08 | 55.6 | 55.6 |
| 16 | 56.30 ^l | 56.66 | 56.62 | 56.73 | 56.69 |
| 17 | 59.00 ^m | 59.74 | 59.28 | 59.42 | 59.73 |
| 18 | 51.43 ^j | 47.46 | 48.46 | 47.38 | 47.56 |
| 19 | 45.60 ⁿ | 44.64 | 46.68 | 44.53 | 44.83 |
| MSE | | 0.01 | -0.14 | -0.42 | 0.07 |
| MAE | | 1.36 | 1.00 | 1.21 | 1.49 |
| RMS | | 1.75 | 1.36 | 1.68 | 1.78 |

^aRef⁹⁴. ^bRef¹⁰¹. ^cRef⁹³. ^dRef¹⁰⁹. ^eRef⁹⁸. ^fRef⁹⁹. ^gRef¹⁰⁰. ^hRef⁹⁵. ⁱRef¹⁰³. ^jRef⁹⁶. ^kRef¹¹⁰. ^lRef¹⁰². ^mRef¹¹¹. ⁿRef¹¹².



Table S3. Logarithm of pre-exponential factors ($\log A/s^{-1}$) of selected gas-phase reactions calculated with RIC. Missing values are caused by the failure in the back-transformation from internal to Cartesian coordinates.

| Rxn | Expt | RIC | | | |
|-----|--------------------|-------|-------|-------------|--------------|
| | | UM-N | UM-VT | E-Optimized | E'-Optimized |
| 1 | 12.70 ^a | - | - | 13.33 | 13.41 |
| 2 | 12.72 ^b | - | - | - | - |
| 3 | 12.54 ^a | - | - | - | 13.44 |
| 4 | 12.78 ^c | - | - | - | 13.55 |
| 5 | 12.57 ^c | - | - | - | 13.53 |
| 6 | 12.84 ^d | - | - | - | 13.32 |
| 7 | 12.56 ^c | - | - | - | - |
| 8 | 12.50 ^e | 13.24 | 12.69 | - | - |
| 9 | 10.67 ^f | 12.17 | 11.22 | 12.19 | 12.78 |
| 10 | 12.25 ^f | 13.3 | 12.51 | 13.09 | 13.64 |
| 11 | 11.23 ^h | 12.24 | 11.36 | - | 13.28 |
| 12 | 10.83 ^f | 12.33 | 11.91 | - | 12.77 |
| 13 | 13.20 ⁱ | - | - | - | 14.33 |
| 14 | 14.29 ^j | 14.42 | 14.6 | 14.32 | 13.88 |
| 15 | 13.45 ^k | 14.46 | 14.02 | 14.47 | 14.22 |
| 16 | 13.33 ^l | 13.83 | 13.85 | 13.85 | 14.05 |
| 17 | 13.90 ^m | 13.96 | 12.52 | 13.87 | 13.69 |
| 18 | 13.81 ^j | 13.75 | 14.02 | 13.77 | 13.94 |
| 19 | 12.56 ⁿ | 13.99 | 14.07 | 13.87 | 13.88 |
| MSE | | 0.81 | 0.36 | 0.64 | 0.92 |
| MAE | | 0.76 | 0.61 | 0.66 | 1.00 |
| RMS | | 0.92 | 0.77 | 0.84 | 1.17 |

^aRef ⁹⁴. ^bRef ¹⁰¹. ^cRef ⁹³. ^dRef ¹⁰⁹. ^eRef ⁹⁸. ^fRef ⁹⁹. ^gRef ¹⁰⁰. ^hRef ⁹⁵. ⁱRef ¹⁰³. ^jRef ⁹⁶. ^kRef ¹¹⁰. ^lRef ¹⁰². ^mRef ¹¹¹. ⁿRef ¹¹².

Table S4. Fundamental frequencies of propanal calculated with different models (cm⁻¹).

| Mode | Expt ¹¹³ | UM-N | UM-VT | UM-T | E-optimized | E'-optimized | HO |
|------|---------------------|--------|--------|--------|-------------|--------------|--------|
| 1 | 2992 | 3179.0 | 3179.0 | 3144.1 | 3000.2 | 2995.5 | 3144.1 |
| 2 | 2981 | 3162.4 | 3162.4 | 3139.8 | 2996.8 | 2994.3 | 3139.8 |
| 3 | 2942 | 3131.9 | 3131.9 | 3121.7 | 2981.9 | 2979.8 | 3121.7 |
| 4 | 2904 | 3012.4 | 3012.4 | 3059.3 | 2970.2 | 2968.1 | 3059.3 |
| 5 | 2895 | 2958.5 | 2958.5 | 3050.3 | 2928.8 | 2928.3 | 3050.3 |
| 6 | 2809 | 2753.5 | 2753.5 | 2883.7 | 2752.4 | 2749.1 | 2883.7 |
| 7 | 1743 | 1831.5 | 1831.5 | 1850.4 | 1831.2 | 1794.9 | 1850.4 |
| 8 | 1460 | 1514.0 | 1514.0 | 1512.3 | 1511.3 | 1394.6 | 1512.3 |
| 9 | 1451 | 1509.2 | 1509.2 | 1505.1 | 1510.8 | 1257.8 | 1505.1 |
| 10 | 1416 | 1473.0 | 1472.9 | 1473.9 | 1473.3 | 1252.7 | 1474.1 |
| 11 | 1390 | 1434.5 | 1434.5 | 1432.7 | 1435.4 | 1252.4 | 1432.7 |
| 12 | 1376 | 1429.1 | 1429.1 | 1418.8 | 1430.8 | 1223.5 | 1418.8 |
| 13 | 1335 | 1330.1 | 1330.0 | 1335.7 | 1320.3 | 1214.3 | 1335.8 |
| 14 | 1250 | 1277.8 | 1277.7 | 1277.7 | 1287.4 | 1196.9 | 1277.7 |
| 15 | 1118 | 1167.8 | 1167.8 | 1166.5 | 1166.4 | 1187.6 | 1166.5 |
| 16 | 1093 | 1145.3 | 1145.2 | 1143.4 | 1146.5 | 1184.3 | 1143.5 |
| 17 | 993 | 1029.7 | 1029.6 | 1029.3 | 1029.1 | 1175.3 | 1029.3 |
| 18 | 892 | 931.9 | 931.2 | 927.9 | 931.3 | 1158.4 | 928.6 |
| 19 | 848 | 883.7 | 883.7 | 883.6 | 885.1 | 1035.7 | 883.6 |
| 20 | 668 | 765.7 | 764.6 | 761.9 | 766.2 | 1012.2 | 762.9 |
| 21 | 660 | 516.1 | 513.9 | 512.2 | 516.8 | 988.0 | 514.6 |
| 22 | 271 | 334.5 | 331.4 | 328.4 | 334.9 | 704.5 | 331.9 |
| 23 | 220 | 203.9 | 152.9 | 152.9 | 205.7 | 554.5 | 210.9 |
| 24 | 135 | 75.4 | 5.9 | 5.9 | 75.8 | 548.9 | 73.1 |
| MSE | | 50.4 | 45.0 | 53.1 | 26.9 | 79.6 | 58.7 |
| MAE | | 73.7 | 78.6 | 81.8 | 50.9 | 158.4 | 76.7 |
| RMS | | 89.8 | 93.7 | 96.5 | 58.4 | 203.2 | 92.7 |



Table S5. Fundamental frequencies of 2-methyl-1-butene calculated with different

models (cm^{-1}).

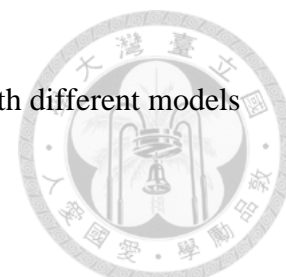
| Mode | Expt ¹¹⁴ | UM-N | UM-VT | UM-T | E-optimized | E'-optimized | HO |
|------|---------------------|--------|--------|--------|-------------|--------------|--------|
| 1 | 3084 | 3151.2 | 3151.2 | 3243.3 | 3025.1 | 3016.7 | 3164.3 |
| 2 | 2994 | 3143.3 | 3143.3 | 3159.4 | 3017.8 | 3016.2 | 3155.6 |
| 3 | 2986 | 3142.7 | 3142.7 | 3140.0 | 3012.0 | 3002.5 | 3140.4 |
| 4 | 2984 | 3140.9 | 3141.0 | 3133.0 | 2996.8 | 2990.7 | 3133.2 |
| 5 | 2976 | 3127.6 | 3127.6 | 3126.7 | 2949.4 | 2943.8 | 3096.4 |
| 6 | 2976 | 3107.1 | 3107.1 | 3095.8 | 2946.6 | 2940.5 | 3091.9 |
| 7 | 2945 | 3099.1 | 3099.1 | 3055.6 | 2945.0 | 2938.7 | 3088.1 |
| 8 | 2943 | 3016.2 | 3016.2 | 3055.1 | 2943.4 | 2938.4 | 3046.4 |
| 9 | 2900 | 3007.5 | 3007.4 | 3040.1 | 2941.6 | 2937.4 | 3041.8 |
| 10 | 2880 | 2995.7 | 2995.7 | 3028.1 | 2939.5 | 2937.2 | 3034.1 |
| 11 | 1644 | 1768.7 | 1768.7 | 1742.1 | 1768.4 | 1670.5 | 1774.0 |
| 12 | 1467 | 1506.3 | 1506.3 | 1517.8 | 1503.6 | 1352.6 | 1503.4 |
| 13 | 1462 | 1505.4 | 1505.4 | 1504.4 | 1502.8 | 1232.3 | 1502.7 |
| 14 | 1460 | 1500.4 | 1500.3 | 1501.2 | 1497.0 | 1227.9 | 1498.9 |
| 15 | 1458 | 1490.9 | 1490.8 | 1488.5 | 1495.4 | 1227.3 | 1487.8 |
| 16 | 1447 | 1487.8 | 1487.8 | 1480.1 | 1491.9 | 1219.4 | 1486.0 |
| 17 | 1414 | 1479.5 | 1479.5 | 1459.3 | 1487.5 | 1215.3 | 1477.8 |
| 18 | 1379 | 1436.7 | 1436.7 | 1422.2 | 1439.6 | 1212.0 | 1431.8 |
| 19 | 1371 | 1429.3 | 1429.3 | 1418.3 | 1436.4 | 1208.8 | 1425.5 |
| 20 | 1329 | 1428.4 | 1428.4 | 1402.3 | 1436.2 | 1206.7 | 1419.7 |
| 21 | 1255 | 1382.5 | 1382.5 | 1309.3 | 1383.8 | 1206.3 | 1379.4 |
| 22 | 1249 | 1248.5 | 1248.5 | 1268.6 | 1248.6 | 1171.8 | 1246.5 |
| 23 | 1089 | 1140.7 | 1140.7 | 1134.4 | 1140.6 | 1164.8 | 1139.5 |
| 24 | 1082 | 1111.5 | 1111.5 | 1111.7 | 1111.6 | 1161.2 | 1112.6 |
| 25 | 1017 | 1076.8 | 1076.8 | 1053.6 | 1076.6 | 1160.1 | 1075.3 |
| 26 | 1017 | 1068.3 | 1068.1 | 1039.8 | 1067.5 | 1157.5 | 1069.0 |
| 27 | 996 | 1020.5 | 1020.5 | 1014.5 | 1020.2 | 1155.4 | 1022.2 |
| 28 | 938 | 977.9 | 977.9 | 964.1 | 977.7 | 1152.7 | 976.5 |
| 29 | 890 | 968.4 | 968.4 | 943.7 | 969.0 | 1149.5 | 967.4 |
| 30 | 790 | 844.2 | 843.7 | 819.6 | 846.1 | 1147.3 | 836.7 |
| 31 | 772 | 779.7 | 779.7 | 793.4 | 779.9 | 1090.1 | 780.5 |

| | | | | | | | |
|-----|-----|-------|-------|-------|-------|--------|-------|
| 32 | 677 | 534.0 | 534.0 | 695.5 | 534.1 | 1068.4 | 532.1 |
| 33 | 495 | 468.3 | 467.0 | 506.7 | 468.3 | 1063.5 | 464.6 |
| 34 | 434 | 396.8 | 396.8 | 446.2 | 397.0 | 907.4 | 394.4 |
| 35 | 400 | 306.0 | 306.0 | 410.1 | 306.0 | 763.1 | 300.1 |
| 36 | 285 | 266.1 | 248.3 | 286.6 | 252.1 | 711.9 | 269.9 |
| 37 | 257 | 181.9 | 123.8 | 123.8 | 187.2 | 644.7 | 184.9 |
| 38 | 170 | 131.1 | 74.7 | 74.7 | 131.8 | 588.4 | 123.6 |
| 39 | 119 | 109.3 | 36.8 | 36.8 | 112.7 | 480.7 | 104.0 |
| MSE | | 49.9 | 44.6 | 51.7 | 19.4 | 85.9 | 49.9 |
| MAE | | 72.7 | 77.9 | 67.6 | 48.3 | 186.2 | 73.8 |
| RMS | | 86.3 | 90.3 | 84.6 | 59.2 | 240.0 | 87.7 |

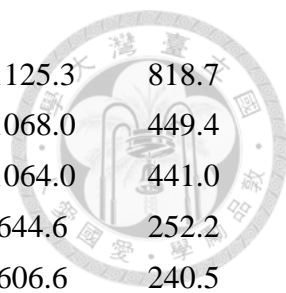
Table S6. Fundamental frequencies of 2-butanone calculated with different models(cm⁻¹).

| Mode | Expt ¹¹⁵ | UM-N | UM-VT | UM-T | E-optimized | E'-optimized | HO |
|------|---------------------|--------|--------|--------|-------------|--------------|--------|
| 1 | 2983 | 3189.8 | 3189.8 | 3177.8 | 3033.0 | 3010.7 | 3177.8 |
| 2 | 2983 | 3180.4 | 3180.4 | 3151.2 | 2998.0 | 2995.6 | 3151.2 |
| 3 | 2983 | 3178.7 | 3178.7 | 3141.4 | 2996.8 | 2992.4 | 3141.4 |
| 4 | 2983 | 3137.7 | 3137.7 | 3124.9 | 2990.7 | 2986.2 | 3124.9 |
| 5 | 2941 | 3127.8 | 3127.8 | 3079.9 | 2983.6 | 2974.3 | 3079.9 |
| 6 | 2910 | 3024.6 | 3024.6 | 3067.7 | 2973.1 | 2950.4 | 3067.7 |
| 7 | 2910 | 3020.9 | 3020.9 | 3058.4 | 2936.0 | 2934.2 | 3058.4 |
| 8 | 2884 | 3004.0 | 3004.0 | 3047.1 | 2932.6 | 2929.8 | 3047.2 |
| 9 | 1716 | 1814.4 | 1814.4 | 1831.7 | 1814.1 | 1786.1 | 1831.7 |
| 10 | 1460 | 1507.9 | 1507.9 | 1504.7 | 1507.5 | 1238.6 | 1504.7 |
| 11 | 1460 | 1502.2 | 1502.1 | 1501.0 | 1502.1 | 1237.7 | 1501.1 |
| 12 | 1422 | 1486.3 | 1486.2 | 1482.0 | 1485.6 | 1232.8 | 1482.1 |
| 13 | 1413 | 1475.5 | 1475.5 | 1474.0 | 1474.7 | 1224.8 | 1474.0 |
| 14 | 1413 | 1457.9 | 1457.9 | 1458.5 | 1458.9 | 1218.1 | 1458.5 |
| 15 | 1373 | 1438.2 | 1438.2 | 1428.0 | 1438.9 | 1212.0 | 1428.0 |
| 16 | 1346 | 1406.7 | 1406.7 | 1402.5 | 1408.1 | 1198.2 | 1402.5 |
| 17 | 1263 | 1382.7 | 1382.7 | 1383.0 | 1382.7 | 1195.1 | 1383.0 |
| 18 | 1263 | 1291.7 | 1291.7 | 1292.9 | 1291.9 | 1171.7 | 1293.0 |
| 19 | 1182 | 1200.3 | 1200.3 | 1199.8 | 1200.4 | 1165.6 | 1199.8 |
| 20 | 1108 | 1140.8 | 1140.5 | 1140.0 | 1140.9 | 1164.8 | 1140.3 |
| 21 | 1089 | 1115.6 | 1115.6 | 1117.8 | 1115.7 | 1161.7 | 1117.8 |
| 22 | 997 | 1015.8 | 1015.8 | 1015.1 | 1016.0 | 1150.1 | 1015.1 |
| 23 | 952 | 960.6 | 959.7 | 960.3 | 960.8 | 1148.7 | 961.1 |
| 24 | 939 | 949.9 | 949.9 | 950.9 | 949.8 | 1135.8 | 950.9 |
| 25 | 768 | 772.5 | 772.5 | 774.2 | 772.2 | 1132.1 | 774.2 |
| 26 | 760 | 765.6 | 764.3 | 759.0 | 766.4 | 1051.8 | 760.2 |
| 27 | 590 | 598.7 | 598.7 | 597.4 | 598.7 | 1035.3 | 597.5 |
| 28 | 460 | 483.9 | 480.2 | 475.0 | 484.2 | 1028.3 | 478.8 |
| 29 | 413 | 408.7 | 408.6 | 408.2 | 408.8 | 906.3 | 408.3 |
| 30 | 260 | 254.5 | 254.4 | 253.3 | 254.5 | 602.4 | 253.4 |

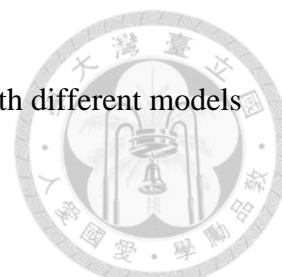
| | | | | | | | |
|-----|-----|-------|------|------|-------|-------|-------|
| 31 | 201 | 196.4 | 89.3 | 89.3 | 190.4 | 597.7 | 214.6 |
| 32 | 106 | 97.0 | 61.0 | 61.0 | 90.0 | 587.6 | 109.0 |
| 33 | 87 | 53.6 | 12.7 | 12.7 | 84.8 | 579.4 | 39.4 |
| MSE | | 61.3 | 55.5 | 54.6 | 31.0 | 100.6 | 60.9 |
| MAE | | 64.8 | 70.1 | 69.4 | 33.4 | 191.5 | 64.5 |
| RMS | | 90.5 | 93.5 | 91.3 | 43.6 | 253.5 | 88.4 |

Table S7. Fundamental frequencies of ethoxy ethane calculated with different models(cm⁻¹).

| Model | Expt ¹¹⁵ | UM-N | UM-VT | UM-T | E-optimized | E'-optimized | HO |
|-------|---------------------|--------|--------|--------|-------------|--------------|--------|
| 1 | 2981 | 3198.9 | 3198.9 | 3145.1 | 2994.7 | 2988.3 | 3145.1 |
| 2 | 2980 | 3191.5 | 3191.5 | 3144.2 | 2994.2 | 2988.2 | 3144.2 |
| 3 | 2953 | 3168.0 | 3168.0 | 3141.5 | 2991.1 | 2987.3 | 3141.5 |
| 4 | 2953 | 3159.7 | 3159.7 | 3140.8 | 2990.5 | 2987.1 | 3140.8 |
| 5 | 2936 | 3069.0 | 3069.0 | 3063.2 | 2985.8 | 2984.6 | 3063.2 |
| 6 | 2935 | 3039.1 | 3039.1 | 3062.6 | 2985.3 | 2983.8 | 3062.6 |
| 7 | 2872 | 3035.4 | 3035.4 | 3009.5 | 2859.1 | 2855.3 | 3009.5 |
| 8 | 2872 | 3034.5 | 3034.5 | 3005.0 | 2858.5 | 2855.2 | 3005.0 |
| 9 | 2862 | 3001.1 | 3001.1 | 2984.5 | 2858.3 | 2854.7 | 2984.5 |
| 10 | 2860 | 2947.7 | 2947.7 | 2974.9 | 2858.2 | 2854.5 | 2975.0 |
| 11 | 1492 | 1540.3 | 1540.3 | 1537.3 | 1538.0 | 1335.5 | 1537.3 |
| 12 | 1481 | 1521.4 | 1521.4 | 1518.6 | 1523.1 | 1332.2 | 1518.6 |
| 13 | 1454 | 1506.9 | 1506.9 | 1505.1 | 1508.0 | 1332.2 | 1505.1 |
| 14 | 1454 | 1504.0 | 1504.0 | 1502.1 | 1507.4 | 1329.2 | 1502.1 |
| 15 | 1453 | 1492.2 | 1492.1 | 1489.5 | 1492.9 | 1279.6 | 1489.5 |
| 16 | 1453 | 1491.6 | 1491.5 | 1488.6 | 1492.0 | 1273.6 | 1488.7 |
| 17 | 1419 | 1459.0 | 1459.0 | 1461.7 | 1458.0 | 1273.5 | 1461.7 |
| 18 | 1381 | 1426.8 | 1426.8 | 1421.8 | 1426.4 | 1261.9 | 1421.8 |
| 19 | 1371 | 1413.4 | 1413.4 | 1408.3 | 1426.3 | 1233.4 | 1408.3 |
| 20 | 1354 | 1387.9 | 1387.9 | 1390.1 | 1388.0 | 1232.7 | 1390.1 |
| 21 | 1278 | 1316.8 | 1316.4 | 1316.7 | 1311.6 | 1217.8 | 1317.1 |
| 22 | 1276 | 1305.5 | 1305.3 | 1305.0 | 1310.8 | 1204.9 | 1305.2 |
| 23 | 1170 | 1207.9 | 1207.8 | 1201.9 | 1204.5 | 1190.5 | 1202.1 |
| 24 | 1144 | 1204.5 | 1204.3 | 1199.3 | 1196.3 | 1185.3 | 1199.3 |
| 25 | 1135 | 1192.8 | 1192.8 | 1193.7 | 1194.5 | 1184.4 | 1193.7 |
| 26 | 1130 | 1175.6 | 1175.6 | 1173.6 | 1176.0 | 1180.1 | 1173.7 |
| 27 | 1078 | 1108.0 | 1108.0 | 1107.6 | 1107.8 | 1175.6 | 1107.6 |
| 28 | 1047 | 1081.8 | 1081.8 | 1079.5 | 1082.1 | 1173.8 | 1079.5 |
| 29 | 923 | 960.5 | 960.5 | 957.9 | 960.4 | 1152.9 | 957.9 |
| 30 | 848 | 875.2 | 875.2 | 874.5 | 875.5 | 1150.3 | 874.5 |
| 31 | 823 | 838.9 | 837.4 | 832.3 | 837.3 | 1125.8 | 833.4 |

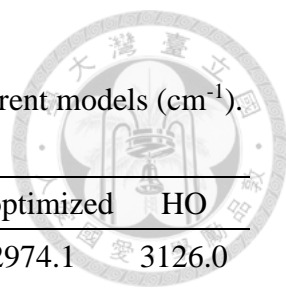


| | | | | | | | |
|-----|-----|-------|-------|-------|-------|--------|-------|
| 32 | 794 | 826.6 | 824.5 | 817.1 | 836.8 | 1125.3 | 818.7 |
| 33 | 443 | 448.8 | 448.8 | 449.4 | 448.8 | 1068.0 | 449.4 |
| 34 | 441 | 443.0 | 443.0 | 441.0 | 443.0 | 1064.0 | 441.0 |
| 35 | 245 | 239.9 | 197.0 | 196.5 | 229.0 | 644.6 | 252.2 |
| 36 | 240 | 237.0 | 134.3 | 134.3 | 223.9 | 606.6 | 240.5 |
| 37 | 230 | 197.1 | 131.5 | 131.5 | 197.2 | 603.6 | 196.5 |
| 38 | 137 | 109.1 | 6.6 | 6.6 | 132.7 | 506.0 | 109.5 |
| 39 | 126 | 98.1 | 3.5 | 3.5 | 123.1 | 497.3 | 76.2 |
| MSE | | 62.3 | 51.8 | 46.0 | 25.7 | 83.5 | 56.4 |
| MAE | | 87.8 | 98.1 | 92.5 | 66.8 | 184.7 | 82.3 |
| RMS | | 100.4 | 110.5 | 104.1 | 82.2 | 240.5 | 92.9 |

Table S8. Fundamental frequencies of 1,4-pentadiene calculated with different models(cm⁻¹).

| Mode | Expt ¹¹⁶ | UM-N | UM-VT | UM-T | E-optimized | E'-optimized | HO |
|------|---------------------|--------|--------|--------|-------------|--------------|--------|
| 1 | 3080 | 3288.2 | 3288.2 | 3242.7 | 3090.2 | 3083.6 | 3242.7 |
| 2 | 3080 | 3280.6 | 3280.6 | 3242.3 | 3084.0 | 3082.8 | 3242.3 |
| 3 | 3012 | 3154.0 | 3154.0 | 3167.6 | 3061.9 | 3058.8 | 3167.6 |
| 4 | 3012 | 3142.6 | 3142.6 | 3166.9 | 3057.4 | 3057.6 | 3166.9 |
| 5 | 3012 | 3140.2 | 3140.2 | 3152.0 | 3035.7 | 3034.4 | 3152.0 |
| 6 | 3012 | 3120.7 | 3120.7 | 3151.2 | 3035.6 | 3034.3 | 3151.2 |
| 7 | 2982 | 3105.7 | 3105.7 | 3086.6 | 2938.4 | 2935.9 | 3086.6 |
| 8 | 2900 | 2976.4 | 2976.4 | 3041.0 | 2936.1 | 2935.5 | 3041.0 |
| 9 | 1644 | 1733.8 | 1733.8 | 1737.8 | 1723.7 | 1623.6 | 1737.8 |
| 10 | 1640 | 1728.8 | 1728.8 | 1724.2 | 1723.6 | 1617.7 | 1724.2 |
| 11 | 1433 | 1483.1 | 1483.1 | 1486.8 | 1482.0 | 1330.7 | 1486.8 |
| 12 | 1413 | 1461.7 | 1461.7 | 1459.9 | 1459.8 | 1314.1 | 1459.9 |
| 13 | 1413 | 1456.0 | 1456.0 | 1454.5 | 1459.4 | 1241.8 | 1454.5 |
| 14 | 1314 | 1338.5 | 1338.5 | 1340.0 | 1333.0 | 1241.5 | 1340.0 |
| 15 | 1295 | 1330.4 | 1330.4 | 1328.7 | 1332.2 | 1233.5 | 1328.7 |
| 16 | 1280 | 1311.8 | 1311.8 | 1315.3 | 1309.6 | 1230.5 | 1315.3 |
| 17 | 1263 | 1271.5 | 1271.5 | 1274.8 | 1273.8 | 1225.6 | 1274.9 |
| 18 | 1120 | 1183.2 | 1183.2 | 1181.6 | 1183.1 | 1222.5 | 1181.6 |
| 19 | 1060 | 1097.2 | 1097.2 | 1097.3 | 1095.7 | 1139.3 | 1097.4 |
| 20 | 995 | 1049.1 | 1049.1 | 1047.5 | 1046.8 | 1128.5 | 1047.5 |
| 21 | 995 | 1043.4 | 1043.4 | 1042.7 | 1045.3 | 1087.2 | 1042.7 |
| 22 | 995 | 981.5 | 981.5 | 979.0 | 989.9 | 1074.0 | 979.1 |
| 23 | 920 | 981.4 | 981.4 | 971.9 | 987.1 | 1034.2 | 971.9 |
| 24 | 918 | 979.9 | 979.9 | 970.8 | 981.5 | 1003.1 | 970.8 |
| 25 | 876 | 925.6 | 925.6 | 924.5 | 925.1 | 943.8 | 924.5 |
| 26 | 760 | 910.5 | 910.4 | 908.3 | 913.0 | 939.3 | 908.3 |
| 27 | 721 | 691.2 | 691.1 | 691.1 | 685.9 | 901.8 | 691.2 |
| 28 | 562 | 626.8 | 625.3 | 624.3 | 633.7 | 884.1 | 625.7 |
| 29 | 421 | 467.4 | 466.5 | 465.2 | 467.5 | 682.6 | 466.4 |
| 30 | 421 | 382.1 | 382.1 | 380.9 | 382.3 | 653.2 | 380.9 |
| 31 | 331 | 305.4 | 301.2 | 299.9 | 305.9 | 598.6 | 304.0 |

| | | | | | | | |
|-----|-----|------|-------|-------|------|-------|------|
| 32 | 137 | 97.8 | 142.1 | 142.1 | 92.0 | 558.4 | 97.4 |
| 33 | 102 | 85.0 | 139.1 | 139.1 | 91.7 | 470.9 | 82.8 |
| MSE | | 61.0 | 63.8 | 64.2 | 31.6 | 75.3 | 61.4 |
| MAE | | 70.9 | 70.6 | 71.3 | 43.9 | 116.6 | 71.8 |
| RMS | | 87.1 | 87.1 | 86.6 | 52.1 | 157.9 | 86.7 |

Table S9. Fundamental frequencies of propane calculated with different models (cm⁻¹).

| Mode | Expt ¹¹⁵ | UM-N | UM-VT | UM-T | E-optimized | E'-optimized | HO |
|------|---------------------|--------|--------|--------|-------------|--------------|--------|
| 1 | 2977 | 3141.4 | 3141.4 | 3126.0 | 2977.4 | 2974.1 | 3126.0 |
| 2 | 2973 | 3140.2 | 3140.2 | 3122.3 | 2974.3 | 2973.9 | 3122.3 |
| 3 | 2968 | 3139.5 | 3139.5 | 3120.8 | 2962.3 | 2958.4 | 3120.8 |
| 4 | 2968 | 3128.4 | 3128.4 | 3109.7 | 2962.3 | 2957.9 | 3109.7 |
| 5 | 2967 | 3110.1 | 3110.1 | 3078.0 | 2961.3 | 2957.7 | 3078.0 |
| 6 | 2962 | 3007.4 | 3007.4 | 3050.1 | 2957.7 | 2956.9 | 3050.1 |
| 7 | 2887 | 3005.7 | 3005.7 | 3046.4 | 2937.9 | 2936.9 | 3046.4 |
| 8 | 2887 | 2989.5 | 2989.5 | 3042.0 | 2937.8 | 2936.7 | 3042.0 |
| 9 | 1476 | 1517.9 | 1517.9 | 1517.5 | 1509.3 | 1283.2 | 1517.5 |
| 10 | 1472 | 1514.3 | 1514.3 | 1511.9 | 1508.5 | 1279.0 | 1511.9 |
| 11 | 1464 | 1503.1 | 1503.1 | 1502.1 | 1506.7 | 1265.5 | 1502.1 |
| 12 | 1462 | 1499.3 | 1499.3 | 1498.3 | 1506.4 | 1258.8 | 1498.3 |
| 13 | 1451 | 1496.3 | 1496.3 | 1493.8 | 1505.5 | 1253.6 | 1493.8 |
| 14 | 1392 | 1432.8 | 1432.8 | 1426.7 | 1434.0 | 1248.1 | 1426.7 |
| 15 | 1378 | 1419.8 | 1419.8 | 1412.7 | 1431.8 | 1238.1 | 1412.7 |
| 16 | 1338 | 1368.4 | 1368.4 | 1372.7 | 1368.1 | 1231.2 | 1372.7 |
| 17 | 1278 | 1321.2 | 1321.1 | 1321.0 | 1321.7 | 1220.5 | 1321.1 |
| 18 | 1192 | 1218.8 | 1218.8 | 1217.6 | 1218.9 | 1216.1 | 1217.6 |
| 19 | 1158 | 1182.9 | 1182.9 | 1185.0 | 1183.0 | 1188.1 | 1185.0 |
| 20 | 1054 | 1080.3 | 1080.3 | 1074.6 | 1080.2 | 1183.3 | 1074.6 |
| 21 | 940 | 940.3 | 940.3 | 939.4 | 939.9 | 1179.5 | 939.5 |
| 22 | 922 | 918.4 | 918.3 | 915.9 | 918.9 | 1178.2 | 916.0 |
| 23 | 869 | 883.5 | 883.5 | 886.0 | 884.0 | 1168.8 | 886.0 |
| 24 | 748 | 766.4 | 763.7 | 753.6 | 766.9 | 1164.4 | 755.8 |
| 25 | 369 | 375.7 | 375.7 | 374.6 | 375.6 | 1031.1 | 374.8 |
| 26 | 268 | 267.5 | 3.1 | 3.1 | 240.1 | 1027.4 | 270.6 |
| 27 | 216 | 219.0 | 0.5 | 0.5 | 234.2 | 670.8 | 218.1 |
| MSE | | 53.4 | 34.7 | 35.3 | 21.9 | 73.3 | 54.0 |
| MAE | | 53.7 | 71.9 | 72.7 | 25.9 | 186.1 | 54.5 |
| RMS | | 75.4 | 100.8 | 101.4 | 31.5 | 269.0 | 76.2 |

Table S10. Fundamental frequencies of propene calculated with different models (cm⁻¹).

| Mode | Expt ¹¹⁶ | UM-N | UM-VT | UM-T | E-optimized | E'-optimized | HO |
|------|---------------------|--------|--------|--------|-------------|--------------|--------|
| 1 | 3090 | 3286.3 | 3286.3 | 3241.8 | 3089.6 | 3083.1 | 3241.8 |
| 2 | 3013 | 3162.9 | 3162.9 | 3165.1 | 3056.4 | 3056.9 | 3165.1 |
| 3 | 2991 | 3134.4 | 3134.4 | 3151.6 | 3031.7 | 3031.0 | 3151.6 |
| 4 | 2954 | 3116.4 | 3116.4 | 3133.4 | 2990.5 | 2985.1 | 3133.4 |
| 5 | 2954 | 3106.1 | 3106.1 | 3106.7 | 2957.6 | 2954.8 | 3106.7 |
| 6 | 2871 | 2999.9 | 2999.9 | 3047.7 | 2955.6 | 2953.9 | 3047.7 |
| 7 | 1650 | 1730.6 | 1730.6 | 1735.7 | 1730.2 | 1631.1 | 1735.7 |
| 8 | 1470 | 1503.7 | 1503.7 | 1501.2 | 1501.5 | 1338.8 | 1501.2 |
| 9 | 1443 | 1488.6 | 1488.6 | 1483.8 | 1488.3 | 1258.9 | 1483.8 |
| 10 | 1420 | 1457.5 | 1457.5 | 1457.5 | 1459.2 | 1233.6 | 1457.5 |
| 11 | 1378 | 1424.9 | 1424.9 | 1413.2 | 1427.1 | 1232.1 | 1413.2 |
| 12 | 1297 | 1337.4 | 1337.4 | 1336.3 | 1337.6 | 1231.8 | 1336.3 |
| 13 | 1171 | 1201.0 | 1201.0 | 1200.3 | 1201.0 | 1227.9 | 1200.3 |
| 14 | 1045 | 1082.0 | 1081.9 | 1079.9 | 1078.4 | 1177.7 | 1080.0 |
| 15 | 991 | 1036.2 | 1036.1 | 1035.7 | 1037.5 | 1153.3 | 1035.7 |
| 16 | 963 | 980.1 | 980.1 | 961.2 | 980.6 | 1131.3 | 961.2 |
| 17 | 920 | 957.8 | 957.8 | 955.3 | 951.1 | 1072.0 | 955.3 |
| 18 | 912 | 932.1 | 932.1 | 935.1 | 940.6 | 980.4 | 935.1 |
| 19 | 578 | 599.8 | 597.0 | 592.3 | 601.4 | 933.1 | 594.9 |
| 20 | 428 | 437.3 | 437.3 | 436.0 | 437.7 | 883.4 | 436.0 |
| 21 | 174 | 189.9 | 23.1 | 23.1 | 193.5 | 757.0 | 202.0 |
| MSE | | 69.1 | 61.1 | 60.9 | 35.0 | 75.9 | 69.6 |
| MAE | | 69.1 | 75.4 | 75.5 | 35.0 | 146.3 | 69.8 |
| RMS | | 90.0 | 95.7 | 98.0 | 40.5 | 207.0 | 92.5 |

Table S11. Fundamental frequencies of butane calculated with different models (cm⁻¹).

| Mode | Expt ¹¹⁵ | UM-N | UM-VT | UM-T | E-optimized | E'-optimized | HO |
|------|---------------------|--------|--------|--------|-------------|--------------|--------|
| 1 | 2968 | 3157.1 | 3157.1 | 3125.0 | 2981.0 | 2975.1 | 3125.0 |
| 2 | 2968 | 3138.1 | 3138.1 | 3124.4 | 2977.6 | 2975.0 | 3124.4 |
| 3 | 2965 | 3135.2 | 3135.2 | 3115.5 | 2963.4 | 2959.5 | 3115.5 |
| 4 | 2965 | 3115.2 | 3115.2 | 3111.8 | 2961.2 | 2959.3 | 3111.8 |
| 5 | 2930 | 3100.2 | 3100.2 | 3081.1 | 2960.2 | 2958.2 | 3081.1 |
| 6 | 2912 | 3085.0 | 3085.0 | 3059.4 | 2958.2 | 2958.1 | 3059.4 |
| 7 | 2872 | 3055.4 | 3055.4 | 3044.5 | 2925.7 | 2924.1 | 3044.5 |
| 8 | 2870 | 3053.1 | 3053.1 | 3044.1 | 2925.5 | 2924.0 | 3044.1 |
| 9 | 2853 | 3020.4 | 3020.4 | 3041.0 | 2925.4 | 2923.9 | 3041.0 |
| 10 | 2853 | 2998.6 | 2998.6 | 3033.8 | 2924.7 | 2923.9 | 3033.8 |
| 11 | 1461 | 1516.9 | 1516.9 | 1517.0 | 1510.8 | 1278.3 | 1517.0 |
| 12 | 1461 | 1511.5 | 1511.5 | 1510.9 | 1510.6 | 1275.2 | 1510.9 |
| 13 | 1461 | 1508.8 | 1508.7 | 1508.2 | 1509.0 | 1269.9 | 1508.2 |
| 14 | 1460 | 1506.9 | 1506.9 | 1506.1 | 1508.7 | 1266.0 | 1506.1 |
| 15 | 1460 | 1498.8 | 1498.8 | 1498.2 | 1501.9 | 1260.2 | 1498.3 |
| 16 | 1442 | 1496.2 | 1496.2 | 1495.8 | 1500.8 | 1258.2 | 1495.8 |
| 17 | 1382 | 1431.0 | 1431.0 | 1423.8 | 1434.2 | 1257.0 | 1423.8 |
| 18 | 1379 | 1425.8 | 1425.8 | 1421.4 | 1433.9 | 1255.9 | 1421.4 |
| 19 | 1361 | 1403.2 | 1403.2 | 1406.9 | 1402.9 | 1233.5 | 1406.9 |
| 20 | 1300 | 1339.0 | 1338.9 | 1339.5 | 1333.2 | 1231.2 | 1339.5 |
| 21 | 1290 | 1327.4 | 1327.4 | 1330.2 | 1332.6 | 1229.6 | 1330.2 |
| 22 | 1257 | 1296.7 | 1296.6 | 1297.2 | 1296.8 | 1229.5 | 1297.3 |
| 23 | 1180 | 1215.5 | 1215.5 | 1214.9 | 1215.6 | 1213.2 | 1214.9 |
| 24 | 1151 | 1178.6 | 1178.6 | 1180.0 | 1178.7 | 1210.6 | 1180.0 |
| 25 | 1059 | 1085.8 | 1085.8 | 1082.7 | 1085.5 | 1178.2 | 1082.7 |
| 26 | 1009 | 1039.5 | 1039.5 | 1034.5 | 1039.4 | 1175.5 | 1034.5 |
| 27 | 964 | 990.8 | 990.8 | 989.5 | 991.5 | 1171.4 | 989.5 |
| 28 | 948 | 971.7 | 971.6 | 971.7 | 971.9 | 1171.4 | 971.8 |
| 29 | 837 | 852.8 | 852.8 | 853.4 | 853.0 | 1168.2 | 853.4 |
| 30 | 803 | 824.7 | 824.6 | 822.4 | 824.5 | 1165.9 | 822.4 |
| 31 | 731 | 751.2 | 748.2 | 739.8 | 752.0 | 1065.4 | 742.6 |
| 32 | 425 | 432.0 | 432.0 | 432.0 | 432.1 | 1035.9 | 432.0 |
| 33 | 271 | 267.2 | 267.1 | 264.7 | 267.4 | 1034.0 | 269.3 |



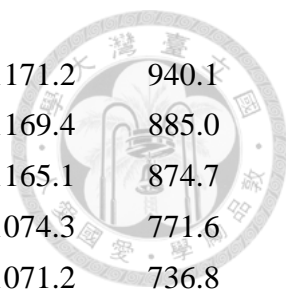
| | | | | | | | |
|-----|-----|-------|-------|-------|-------|-------|-------|
| 34 | 225 | 253.1 | 164.8 | 164.8 | 231.2 | 606.8 | 264.9 |
| 35 | 194 | 221.9 | 13.6 | 13.6 | 229.7 | 590.2 | 237.0 |
| 36 | 102 | 120.7 | 3.6 | 3.6 | 127.5 | 588.6 | 121.9 |
| MSE | | 71.0 | 59.4 | 56.5 | 33.6 | 87.0 | 69.0 |
| MAE | | 71.2 | 78.5 | 75.7 | 34.1 | 180.4 | 69.1 |
| RMS | | 95.0 | 101.2 | 97.4 | 39.0 | 251.6 | 91.3 |

Table S12. Fundamental frequencies of 1-butene calculated with different models (cm⁻¹).

| Mode | Expt ¹¹⁶ | UM-N | UM-VT | UM-T | E-optimized | E'-optimized | HO |
|------|---------------------|--------|--------|--------|-------------|--------------|--------|
| 1 | 3086 | 3277.8 | 3277.8 | 3239.8 | 3082.1 | 3080.8 | 3239.8 |
| 2 | 2998 | 3177.0 | 3177.0 | 3155.2 | 3059.7 | 3057.0 | 3155.2 |
| 3 | 2998 | 3165.7 | 3165.7 | 3144.9 | 3019.9 | 3018.7 | 3144.9 |
| 4 | 2970 | 3159.9 | 3159.9 | 3132.4 | 2981.9 | 2977.6 | 3132.4 |
| 5 | 2970 | 3104.6 | 3104.6 | 3123.8 | 2975.0 | 2973.6 | 3123.8 |
| 6 | 2925 | 3099.3 | 3099.3 | 3086.1 | 2967.6 | 2964.2 | 3086.1 |
| 7 | 2908 | 3005.9 | 3005.9 | 3050.3 | 2951.2 | 2950.2 | 3050.3 |
| 8 | 2851 | 2969.3 | 2969.3 | 3043.5 | 2924.0 | 2922.0 | 3043.5 |
| 9 | 1645 | 1727.5 | 1727.5 | 1733.0 | 1727.4 | 1619.7 | 1733.0 |
| 10 | 1457 | 1513.4 | 1513.3 | 1512.3 | 1512.2 | 1338.3 | 1512.3 |
| 11 | 1457 | 1506.5 | 1506.5 | 1502.1 | 1506.9 | 1260.2 | 1502.1 |
| 12 | 1450 | 1492.1 | 1492.1 | 1492.8 | 1492.7 | 1257.2 | 1492.8 |
| 13 | 1420 | 1462.9 | 1462.9 | 1462.7 | 1462.8 | 1251.2 | 1462.8 |
| 14 | 1390 | 1430.7 | 1430.7 | 1417.7 | 1430.9 | 1250.4 | 1417.7 |
| 15 | 1307 | 1349.8 | 1349.8 | 1356.1 | 1346.9 | 1249.8 | 1356.1 |
| 16 | 1294 | 1331.2 | 1331.2 | 1329.1 | 1332.2 | 1236.9 | 1329.1 |
| 17 | 1264 | 1297.1 | 1297.1 | 1298.5 | 1297.7 | 1226.8 | 1298.6 |
| 18 | 1174 | 1210.9 | 1210.9 | 1209.7 | 1211.0 | 1215.4 | 1209.8 |
| 19 | 1073 | 1104.0 | 1104.0 | 1104.8 | 1102.4 | 1212.2 | 1104.8 |
| 20 | 1020 | 1049.3 | 1049.2 | 1048.3 | 1046.8 | 1183.2 | 1048.3 |
| 21 | 993 | 1038.3 | 1038.3 | 1036.1 | 1041.6 | 1170.4 | 1036.2 |
| 22 | 980 | 1000.8 | 1000.7 | 999.3 | 1001.3 | 1159.2 | 999.3 |
| 23 | 912 | 982.8 | 982.8 | 964.8 | 982.2 | 1100.7 | 964.8 |
| 24 | 853 | 869.2 | 869.1 | 869.9 | 869.4 | 1017.5 | 869.9 |
| 25 | 788 | 811.0 | 810.5 | 805.4 | 811.5 | 938.8 | 805.8 |
| 26 | 623 | 663.8 | 662.4 | 659.8 | 663.7 | 897.0 | 661.2 |
| 27 | 437 | 443.9 | 439.8 | 440.5 | 443.9 | 886.4 | 444.8 |
| 28 | 320 | 324.6 | 323.2 | 320.5 | 325.1 | 704.4 | 322.0 |
| 29 | 282 | 223.7 | 35.7 | 35.7 | 224.2 | 623.8 | 227.6 |
| 30 | 237 | 106.3 | 6.5 | 6.5 | 108.7 | 573.3 | 112.6 |
| MSE | | 60.6 | 50.7 | 50.0 | 27.4 | 74.5 | 60.2 |
| MAE | | 73.2 | 82.5 | 81.8 | 40.0 | 141.1 | 72.1 |
| RMS | | 93.2 | 108.6 | 107.9 | 47.7 | 183.5 | 92.0 |

Table S13. Fundamental frequencies of pentane calculated with different models (cm⁻¹).

| Mode | Expt ¹¹⁶ | UM-N | UM-VT | UM-T | E-optimized | E'-optimized | HO |
|------|---------------------|--------|--------|--------|-------------|--------------|--------|
| 1 | 2973 | 3157.6 | 3157.6 | 3127.8 | 2979.2 | 2974.9 | 3127.8 |
| 2 | 2967 | 3157.0 | 3157.0 | 3126.4 | 2976.3 | 2974.1 | 3126.4 |
| 3 | 2965 | 3117.8 | 3117.8 | 3119.3 | 2965.8 | 2959.6 | 3119.3 |
| 4 | 2965 | 3115.7 | 3115.7 | 3116.4 | 2961.9 | 2959.4 | 3116.4 |
| 5 | 2930 | 3097.3 | 3097.3 | 3086.1 | 2959.7 | 2958.8 | 3086.1 |
| 6 | 2930 | 3093.7 | 3093.7 | 3071.7 | 2959.6 | 2958.3 | 3071.7 |
| 7 | 2908 | 3079.2 | 3079.2 | 3051.6 | 2926.9 | 2925.4 | 3051.6 |
| 8 | 2892 | 3060.7 | 3060.7 | 3048.9 | 2926.6 | 2925.0 | 3048.9 |
| 9 | 2879 | 3017.9 | 3017.9 | 3046.5 | 2925.9 | 2924.4 | 3046.5 |
| 10 | 2866 | 3007.5 | 3007.5 | 3044.2 | 2925.6 | 2924.2 | 3044.2 |
| 11 | 2866 | 3005.4 | 3005.4 | 3038.7 | 2912.6 | 2910.4 | 3038.7 |
| 12 | 2866 | 2971.2 | 2971.2 | 3025.5 | 2911.9 | 2910.0 | 3025.5 |
| 13 | 1480 | 1517.6 | 1517.6 | 1517.7 | 1510.0 | 1263.5 | 1517.7 |
| 14 | 1476 | 1511.0 | 1511.0 | 1510.3 | 1508.7 | 1261.3 | 1510.3 |
| 15 | 1469 | 1506.4 | 1506.4 | 1504.2 | 1508.3 | 1259.7 | 1504.2 |
| 16 | 1463 | 1506.3 | 1506.3 | 1503.5 | 1508.1 | 1259.0 | 1503.5 |
| 17 | 1462 | 1503.4 | 1503.4 | 1501.1 | 1504.0 | 1256.9 | 1501.1 |
| 18 | 1456 | 1495.2 | 1495.2 | 1494.5 | 1501.0 | 1255.6 | 1494.5 |
| 19 | 1450 | 1494.0 | 1494.0 | 1493.3 | 1498.3 | 1251.1 | 1493.3 |
| 20 | 1389 | 1429.1 | 1429.1 | 1423.3 | 1434.2 | 1250.8 | 1423.3 |
| 21 | 1379 | 1426.6 | 1426.6 | 1419.4 | 1433.5 | 1249.8 | 1419.4 |
| 22 | 1379 | 1414.4 | 1414.4 | 1417.4 | 1413.2 | 1239.2 | 1417.4 |
| 23 | 1346 | 1375.2 | 1375.2 | 1378.6 | 1375.4 | 1238.7 | 1378.6 |
| 24 | 1346 | 1339.2 | 1339.2 | 1339.8 | 1336.9 | 1233.8 | 1339.9 |
| 25 | 1303 | 1334.5 | 1334.4 | 1334.4 | 1335.9 | 1231.9 | 1334.5 |
| 26 | 1269 | 1298.1 | 1298.1 | 1300.4 | 1298.6 | 1231.7 | 1300.4 |
| 27 | 1269 | 1273.0 | 1273.0 | 1273.1 | 1273.1 | 1224.9 | 1273.2 |
| 28 | 1170 | 1211.7 | 1211.7 | 1211.5 | 1211.8 | 1214.1 | 1211.5 |
| 29 | 1144 | 1172.8 | 1172.8 | 1173.5 | 1172.8 | 1211.5 | 1173.5 |
| 30 | 1073 | 1097.0 | 1097.0 | 1093.4 | 1097.0 | 1202.2 | 1093.4 |
| 31 | 1036 | 1065.0 | 1065.0 | 1064.1 | 1058.3 | 1177.3 | 1064.1 |
| 32 | 1024 | 1052.6 | 1052.6 | 1051.0 | 1056.4 | 1176.0 | 1051.0 |
| 33 | 993 | 1001.9 | 1001.8 | 1001.5 | 1001.9 | 1171.4 | 1001.6 |



| | | | | | | | |
|-----|-----|-------|-------|-------|-------|--------|-------|
| 34 | 910 | 942.2 | 942.2 | 940.1 | 941.5 | 1171.2 | 940.1 |
| 35 | 867 | 885.9 | 885.9 | 885.0 | 886.8 | 1169.4 | 885.0 |
| 36 | 858 | 876.7 | 876.7 | 874.6 | 876.8 | 1165.1 | 874.7 |
| 37 | 766 | 776.6 | 775.6 | 770.7 | 766.1 | 1074.3 | 771.6 |
| 38 | 727 | 744.8 | 742.5 | 734.6 | 761.7 | 1071.2 | 736.8 |
| 39 | 406 | 405.9 | 405.9 | 404.9 | 405.8 | 1041.3 | 404.9 |
| 40 | 401 | 404.7 | 404.7 | 403.5 | 404.7 | 1034.6 | 403.5 |
| 41 | 215 | 244.2 | 180.7 | 179.7 | 228.5 | 651.6 | 242.7 |
| 42 | 210 | 235.0 | 153.2 | 153.2 | 224.1 | 603.6 | 233.2 |
| 43 | 179 | 180.7 | 146.0 | 146.0 | 180.9 | 600.9 | 179.6 |
| 44 | 131 | 109.4 | 13.6 | 13.6 | 131.7 | 588.1 | 106.3 |
| 45 | 88 | 102.2 | 2.4 | 2.4 | 113.7 | 461.3 | 89.8 |
| MSE | | 59.4 | 51.0 | 50.6 | 25.6 | 81.3 | 58.6 |
| MAE | | 60.7 | 65.8 | 65.5 | 26.1 | 180.8 | 60.0 |
| RMS | | 85.2 | 88.3 | 88.4 | 30.9 | 242.3 | 85.2 |



References

- (1) Jacobs, P.; Flanigen, E. M.; Jansen, J.; van Bekkum, H. *Introduction to zeolite science and practice*; Elsevier, 2001.
- (2) Komvokis, V.; Tan, L. X. L.; Clough, M.; Pan, S. S.; Yilmaz, B. Zeolites in fluid catalytic cracking (FCC). *Zeolites in Sustainable Chemistry: Synthesis, Characterization and Catalytic Applications* **2016**, 271-297.
- (3) Zhang, Q.; Yu, J.; Corma, A. Applications of zeolites to C1 chemistry: recent advances, challenges, and opportunities. *Advanced Materials* **2020**, 32 (44), 2002927.
- (4) Ackley, M. W.; Rege, S. U.; Saxena, H. Application of natural zeolites in the purification and separation of gases. *Microporous and Mesoporous Materials* **2003**, 61 (1-3), 25-42.
- (5) Kosinov, N.; Gascon, J.; Kapteijn, F.; Hensen, E. J. Recent developments in zeolite membranes for gas separation. *Journal of Membrane Science* **2016**, 499, 65-79.
- (6) Ennaert, T.; Van Aelst, J.; Dijkmans, J.; De Clercq, R.; Schutyser, W.; Dusselier, M.; Verboekend, D.; Sels, B. F. Potential and challenges of zeolite chemistry in the catalytic conversion of biomass. *Chemical Society Reviews* **2016**, 45 (3), 584-611.
- (7) Li, Y.; Li, L.; Yu, J. Applications of zeolites in sustainable chemistry. *Chem* **2017**, 3 (6), 928-949.
- (8) Li, Y.-P.; Head-Gordon, M.; Bell, A. T. Analysis of the reaction mechanism and catalytic activity of metal-substituted beta zeolite for the isomerization of glucose to fructose. *Acs Catalysis* **2014**, 4 (5), 1537-1545.
- (9) Li, K.; Valla, J.; Garcia-Martinez, J. Realizing the commercial potential of hierarchical zeolites: new opportunities in catalytic cracking. *ChemCatChem* **2014**, 6 (1), 46-66.
- (10) Mallikarjun Sharada, S.; Zimmerman, P. M.; Bell, A. T.; Head-Gordon, M. Insights into the kinetics of cracking and dehydrogenation reactions of light alkanes in H-MFI. *The Journal of Physical Chemistry C* **2013**, 117 (24), 12600-12611.
- (11) Stöcker, M. Gas phase catalysis by zeolites. *Microporous and Mesoporous Materials* **2005**, 82 (3), 257-292.
- (12) Tranca, D. C.; Zimmerman, P. M.; Gomes, J.; Lambrecht, D.; Keil, F. J.; Head-Gordon, M.; Bell, A. T. Hexane cracking on ZSM-5 and faujasite

zeolites: a QM/MM/QCT study. *The Journal of Physical Chemistry C* **2015**, *119* (52), 28836-28853.

(13) Bender, M. An overview of industrial processes for the production of olefins–C4 hydrocarbons. *ChemBioEng Reviews* **2014**, *1* (4), 136-147.

(14) Janda, A.; Bell, A. T. Effects of Si/Al ratio on the distribution of framework Al and on the rates of alkane monomolecular cracking and dehydrogenation in H-MFI. *Journal of the American Chemical Society* **2013**, *135* (51), 19193-19207.

(15) Jones, A. J.; Zones, S. I.; Iglesia, E. Implications of transition state confinement within small voids for acid catalysis. *The Journal of Physical Chemistry C* **2014**, *118* (31), 17787-17800.

(16) Lin, L.; Qiu, C.; Zhuo, Z.; Zhang, D.; Zhao, S.; Wu, H.; Liu, Y.; He, M. Acid strength controlled reaction pathways for the catalytic cracking of 1-butene to propene over ZSM-5. *Journal of catalysis* **2014**, *309*, 136-145.

(17) Niwa, M.; Suzuki, K.; Morishita, N.; Sastre, G.; Okumura, K.; Katada, N. Dependence of cracking activity on the Brønsted acidity of Y zeolite: DFT study and experimental confirmation. *Catalysis Science & Technology* **2013**, *3* (8), 1919-1927.

(18) Xu, B.; Sievers, C.; Hong, S. B.; Prins, R.; van Bokhoven, J. A. Catalytic activity of Brønsted acid sites in zeolites: Intrinsic activity, rate-limiting step, and influence of the local structure of the acid sites. *Journal of Catalysis* **2006**, *244* (2), 163-168.

(19) Wang, S.; He, Y.; Jiao, W.; Wang, J.; Fan, W. Recent experimental and theoretical studies on Al siting/acid site distribution in zeolite framework. *Current Opinion in Chemical Engineering* **2019**, *23*, 146-154.

(20) Yang, C.-T.; Janda, A.; Bell, A. T.; Lin, L.-C. Atomistic investigations of the effects of Si/Al ratio and Al distribution on the adsorption selectivity of n-alkanes in Brønsted-acid zeolites. *The Journal of Physical Chemistry C* **2018**, *122* (17), 9397-9410.

(21) Janda, A.; Vlaisavljevich, B.; Lin, L.-C.; Mallikarjun Sharada, S.; Smit, B.; Head-Gordon, M.; Bell, A. T. Adsorption thermodynamics and intrinsic activation parameters for monomolecular cracking of n-alkanes on Brønsted acid sites in zeolites. *The Journal of Physical Chemistry C* **2015**, *119* (19), 10427-10438.

(22) Hohenberg, P.; Kohn, W. Inhomogeneous electron gas. *Physical review* **1964**, *136* (3B), B864.

- 
- (23) Kohn, W.; Sham, L. J. Self-consistent equations including exchange and correlation effects. *Physical review* **1965**, *140* (4A), A1133.
- (24) Bursch, M.; Mewes, J. M.; Hansen, A.; Grimme, S. Best-Practice DFT Protocols for Basic Molecular Computational Chemistry. *Angewandte Chemie International Edition* **2022**, *61* (42), e202205735.
- (25) Mace, A.; Laasonen, K.; Laaksonen, A. Free energy barriers for CO₂ and N₂ in zeolite NaKA: an ab initio molecular dynamics approach. *Physical Chemistry Chemical Physics* **2014**, *16* (1), 166-172.
- (26) Piccini, G.; Sauer, J. Quantum chemical free energies: Structure optimization and vibrational frequencies in normal modes. *Journal of chemical theory and computation* **2013**, *9* (11), 5038-5045.
- (27) Amsler, J.; Plessow, P. N.; Studt, F.; Bučko, T. s. Anharmonic Correction to Free Energy Barriers from DFT-Based Molecular Dynamics Using Constrained Thermodynamic Integration. *Journal of Chemical Theory and Computation* **2023**.
- (28) Rybicki, M.; Sauer, J. Rigid Body Approximation for the Anharmonic Description of Molecule–Surface Vibrations. *Journal of Chemical Theory and Computation* **2022**, *18* (9), 5618-5635.
- (29) Meng, Q.; Zhang, L.; Chen, Q.; Chi, Y.; Zhang, P. Influence of torsional anharmonicity on the reactions of methyl butanoate with hydroperoxyl radical. *The Journal of Physical Chemistry A* **2020**, *124* (42), 8643-8652.
- (30) Zheng, J.; Truhlar, D. G. Quantum thermochemistry: Multistructural method with torsional anharmonicity based on a coupled torsional potential. *Journal of Chemical Theory and Computation* **2013**, *9* (3), 1356-1367.
- (31) Piccini, G.; Alessio, M.; Sauer, J.; Zhi, Y.; Liu, Y.; Kolvenbach, R.; Jentys, A.; Lercher, J. A. Accurate adsorption thermodynamics of small alkanes in zeolites. Ab initio theory and experiment for H-chabazite. *The Journal of Physical Chemistry C* **2015**, *119* (11), 6128-6137.
- (32) Piccini, G.; Sauer, J. Effect of anharmonicity on adsorption thermodynamics. *Journal of chemical theory and computation* **2014**, *10* (6), 2479-2487.
- (33) Zapata Trujillo, J. C.; McKemmish, L. K. Model chemistry recommendations for scaled harmonic frequency calculations: A benchmark study. *The Journal of Physical Chemistry A* **2023**, *127* (7), 1715-1735.
- (34) Spicher, S.; Grimme, S. Efficient computation of free energy contributions for association reactions of large molecules. *The Journal of*

Physical Chemistry Letters **2020**, *11* (16), 6606-6611.

(35) Rauhut, G.; Knizia, G.; Werner, H.-J. Accurate calculation of vibrational frequencies using explicitly correlated coupled-cluster theory. *The Journal of chemical physics* **2009**, *130* (5), 054105.

(36) Besler, B. H.; Scuseria, G. E.; Scheiner, A. C.; Schaefer III, H. F. A systematic theoretical study of harmonic vibrational frequencies: The single and double excitation coupled cluster (CCSD) method. *The Journal of chemical physics* **1988**, *89* (1), 360-366.

(37) Christiansen, O. Vibrational coupled cluster theory. *The Journal of chemical physics* **2004**, *120* (5), 2149-2159.

(38) Bowman, J. M. The self-consistent-field approach to polyatomic vibrations. *Accounts of Chemical Research* **1986**, *19* (7), 202-208.

(39) Gerber, R.; Ratner, M. A. Self-consistent-field methods for vibrational excitations in polyatomic systems. *Advances in Chemical Physics: Evolution of Size Effects in Chemical Dynamics* **1988**, (Part 1), 97-132.

(40) Bowman, J. M. Self-consistent field energies and wavefunctions for coupled oscillators. *The Journal of Chemical Physics* **1978**, *68* (2), 608-610.

(41) Barone, V. Anharmonic vibrational properties by a fully automated second-order perturbative approach. *The Journal of chemical physics* **2005**, *122* (1), 014108.

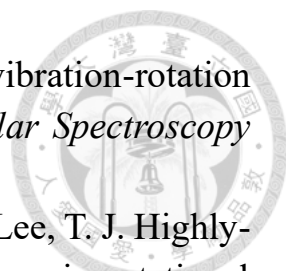
(42) Wilson Jr, E. B.; Howard, J. The vibration-rotation energy levels of polyatomic molecules I. Mathematical theory of semirigid asymmetrical top molecules. *The Journal of Chemical Physics* **1936**, *4* (4), 260-268.

(43) Franke, P. R.; Stanton, J. F.; Doublerly, G. E. How to VPT2: accurate and intuitive simulations of CH stretching infrared spectra using VPT2+ K with large effective Hamiltonian resonance treatments. *The Journal of Physical Chemistry A* **2021**, *125* (6), 1301-1324.

(44) Bowman, J. M.; Christoffel, K.; Tobin, F. Application of SCF-SI theory to vibrational motion in polyatomic molecules. *Journal of Physical Chemistry* **1979**, *83* (8), 905-912.

(45) Carter, S.; Bowman, J. M.; Handy, N. C. Extensions and tests of "multimode": a code to obtain accurate vibration/rotation energies of many-mode molecules. *Theoretical Chemistry Accounts* **1998**, *100*, 191-198.

(46) Christoffel, K. M.; Bowman, J. M. Investigations of self-consistent field, scf ci and virtual stateconfiguration interaction vibrational energies for a model three-mode system. *Chemical Physics Letters* **1982**, *85* (2), 220-224.

- 
- (47) Whitehead, R.; Handy, N. Variational calculation of vibration-rotation energy levels for triatomic molecules. *Journal of Molecular Spectroscopy* **1975**, *55* (1-3), 356-373.
- (48) Gardner, M. B.; Westbrook, B. R.; Fortenberry, R. C.; Lee, T. J. Highly-accurate quartic force fields for the prediction of anharmonic rotational constants and fundamental vibrational frequencies. *Spectrochimica Acta Part A: Molecular and Biomolecular Spectroscopy* **2021**, *248*, 119184.
- (49) Ermiş, B.; Ünal, A.; Soydaş, E.; Bozkaya, U. Anharmonic force field from coupled-cluster methods and accurate computation of infrared spectra. In *Advances in Quantum Chemistry*, Vol. 83; Elsevier, 2021; pp 139-153.
- (50) Bac, S.; Patra, A.; Kron, K. J.; Mallikarjun Sharada, S. Recent Advances toward Efficient Calculation of Higher Nuclear Derivatives in Quantum Chemistry. *The Journal of Physical Chemistry A* **2022**, *126* (43), 7795-7805.
- (51) Kirchner, B.; Blasius, J.; Esser, L.; Reckien, W. Predicting Vibrational Spectroscopy for Flexible Molecules and Molecules with Non-Idle Environments. *Advanced Theory and Simulations* **2021**, *4* (4), 2000223.
- (52) Le Barbu-Debus, K.; Bowles, J.; Jähnigen, S.; Clavaguéra, C.; Calvo, F.; Vuilleumier, R.; Zehnacker, A. Assessing cluster models of solvation for the description of vibrational circular dichroism spectra: synergy between static and dynamic approaches. *Physical Chemistry Chemical Physics* **2020**, *22* (45), 26047-26068.
- (53) Hudecová, J.; Hopmann, K. H.; Bour, P. Correction of vibrational broadening in molecular dynamics clusters with the normal mode optimization method. *The Journal of Physical Chemistry B* **2012**, *116* (1), 336-342.
- (54) Li, Y.-P.; Bell, A. T.; Head-Gordon, M. Thermodynamics of anharmonic systems: Uncoupled mode approximations for molecules. *Journal of chemical theory and computation* **2016**, *12* (6), 2861-2870.
- (55) Zimmerman, P. M.; Smereka, P. Optimizing vibrational coordinates to modulate intermode coupling. *Journal of chemical theory and computation* **2016**, *12* (4), 1883-1891.
- (56) Peng, C.; Ayala, P. Y.; Schlegel, H. B.; Frisch, M. J. Using redundant internal coordinates to optimize equilibrium geometries and transition states. *Journal of Computational Chemistry* **1996**, *17* (1), 49-56.
- (57) Wang, L.-P.; Song, C. Geometry optimization made simple with translation and rotation coordinates. *The Journal of chemical physics* **2016**,

144 (21), 214108.

(58) Billeter, S. R.; Turner, A. J.; Thiel, W. Linear scaling geometry optimisation and transition state search in hybrid delocalised internal coordinates. *Physical Chemistry Chemical Physics* **2000**, 2 (10), 2177-2186.

(59) Hao, J.; Cheng, D.-g.; Chen, F.; Zhan, X. n-Heptane catalytic cracking on ZSM-5 zeolite nanosheets: Effect of nanosheet thickness. *Microporous and Mesoporous Materials* **2021**, 310, 110647.

(60) Fu, J.; Feng, X.; Liu, Y.; Shan, H.; Yang, C. Mechanistic insights into the pore confinement effect on bimolecular and monomolecular cracking mechanisms of n-octane over HY and HZSM-5 zeolites: A DFT study. *The Journal of Physical Chemistry C* **2018**, 122 (23), 12222-12230.

(61) Inagaki, S.; Shinoda, S.; Hayashi, S.; Wakihara, T.; Yamazaki, H.; Kondo, J. N.; Kubota, Y. Improvement in the catalytic properties of ZSM-5 zeolite nanoparticles via mechanochemical and chemical modifications. *Catalysis Science & Technology* **2016**, 6 (8), 2598-2604.

(62) De Moor, B. A.; Reyniers, M.-F.; Gobin, O. C.; Lercher, J. A.; Marin, G. B. Adsorption of C₂–C₈ n-Alkanes in Zeolites. *The Journal of Physical Chemistry C* **2011**, 115 (4), 1204-1219.

(63) Konno, H.; Okamura, T.; Kawahara, T.; Nakasaka, Y.; Tago, T.; Masuda, T. Kinetics of n-hexane cracking over ZSM-5 zeolites—effect of crystal size on effectiveness factor and catalyst lifetime. *Chemical Engineering Journal* **2012**, 207, 490-496.

(64) Li, S.-C.; Lin, Y.-C.; Li, Y.-P. Comparative analysis of uncoupled mode approximations for molecular thermochemistry and kinetics. *Journal of Chemical Theory and Computation* **2022**, 18 (11), 6866-6877.

(65) Njegic, B.; Gordon, M. S. Predicting accurate vibrational frequencies for highly anharmonic systems. *The Journal of chemical physics* **2008**, 129 (16), 164107.

(66) Shor, A. M.; Shor, E. A. I.; Laletina, S.; Nasluzov, V. A.; Vayssilov, G. N.; Rösch, N. Effect of the size of the quantum region in a hybrid embedded-cluster scheme for zeolite systems. *Chemical Physics* **2009**, 363 (1-3), 33-41.

(67) Zimmerman, P. M.; Head-Gordon, M.; Bell, A. T. Selection and validation of charge and Lennard-Jones parameters for QM/MM simulations of hydrocarbon interactions with zeolites. *Journal of chemical theory and computation* **2011**, 7 (6), 1695-1703.

(68) Olson, D. H.; Khosrovani, N.; Peters, A. W.; Toby, B. H. Crystal

structure of dehydrated CsZSM-5 (5.8 Al): evidence for nonrandom aluminum distribution. *The Journal of Physical Chemistry B* **2000**, *104* (20), 4844-4848.

(69) Mentzen, B.; Sacerdote-Peronnet, M. Prediction of preferred proton locations in HMFI/benzene complexes by molecular mechanics calculations. Comparison with NMR, structural and calorimetric results. *Materials research bulletin* **1994**, *29* (12), 1341-1348.

(70) Foloppe, N.; MacKerell, J., Alexander D. All-atom empirical force field for nucleic acids: I. Parameter optimization based on small molecule and condensed phase macromolecular target data. *Journal of computational chemistry* **2000**, *21* (2), 86-104.

(71) Vanommeslaeghe, K.; Hatcher, E.; Acharya, C.; Kundu, S.; Zhong, S.; Shim, J.; Darian, E.; Guvench, O.; Lopes, P.; Vorobyov, I. CHARMM general force field: A force field for drug-like molecules compatible with the CHARMM all-atom additive biological force fields. *Journal of computational chemistry* **2010**, *31* (4), 671-690.

(72) Yin, D.; MacKerell Jr, A. D. Combined ab initio/empirical approach for optimization of Lennard–Jones parameters. *Journal of Computational Chemistry* **1998**, *19* (3), 334-348.

(73) Li, Y.-P.; Gomes, J.; Mallikarjun Sharada, S.; Bell, A. T.; Head-Gordon, M. Improved force-field parameters for QM/MM simulations of the energies of adsorption for molecules in zeolites and a free rotor correction to the rigid rotor harmonic oscillator model for adsorption enthalpies. *The Journal of Physical Chemistry C* **2015**, *119* (4), 1840-1850.

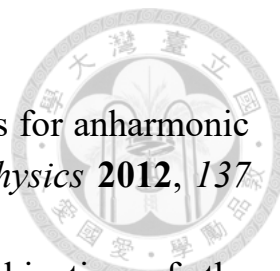
(74) Chai, J.-D.; Head-Gordon, M. Long-range corrected hybrid density functionals with damped atom–atom dispersion corrections. *Physical Chemistry Chemical Physics* **2008**, *10* (44), 6615-6620.

(75) Chai, J.-D.; Head-Gordon, M. Systematic optimization of long-range corrected hybrid density functionals. *The Journal of chemical physics* **2008**, *128* (8), 084106.

(76) Behn, A.; Zimmerman, P. M.; Bell, A. T.; Head-Gordon, M. Efficient exploration of reaction paths via a freezing string method. *The Journal of chemical physics* **2011**, *135* (22), 224108.

(77) Epifanovsky, E.; Gilbert, A. T.; Feng, X.; Lee, J.; Mao, Y.; Mardirossian, N.; Pokhilko, P.; White, A. F.; Coons, M. P.; Dempwolff, A. L. Software for the frontiers of quantum chemistry: An overview of developments in the Q-

- Chem 5 package. *The Journal of chemical physics* **2021**, 155 (8), 084801.
- (78) Johnson, R. D. NIST computational chemistry comparison and benchmark database. <http://srdata.nist.gov/cccbdb> **2006**.
- (79) Johnson III, R. D. NIST computational chemistry comparison and benchmark database, NIST standard reference database number 101. *Release 16a* <http://cccbdb.nist.gov/>(accessed Mar 13, 2015) **2013**.
- (80) Scott, D. Correlation of the chemical thermodynamic properties of alkane hydrocarbons. *The Journal of Chemical Physics* **1974**, 60 (8), 3144-3165.
- (81) Dailey, B. P.; Felsing, W. Heat Capacities of and Hindered Rotation in n-Butane and Isobutane¹. *Journal of the American Chemical Society* **1943**, 65 (1), 44-46.
- (82) Wacker, P.; Cheney, R. K.; Scott, R. Heat capacities of gaseous oxygen, isobutane, and 1-butene from - 30 degrees to + 90 degrees C. *Journal of research of the National Bureau of Standards* **1947**, 38 (6), 651-659.
- (83) Ernst, G.; Büsser, J. Ideal and real gas state heat capacities Cp of C₃H₈, i-C₄H₁₀, CH₂ClCF₃, CF₂ClCFCl₂, and CHF₂Cl. *The Journal of Chemical Thermodynamics* **1970**, 2 (6), 787-791.
- (84) Scott, R. B.; Mellors, J. W. Specific heats of gaseous 1, 3-butadiene, isobutene, styrene, and ethylbenzene. *J. Research Nat. Bur. Stand.* **1945**, 34, 243.
- (85) Bier, K.; Ernst, G.; Kunze, J.; Maurer, G. Thermodynamic properties of propylene from calorimetric measurements. *The Journal of Chemical Thermodynamics* **1974**, 6 (11), 1039-1052.
- (86) Scott, D.; Waddington, G.; Smith, J.; Huffman, H. Thermodynamic properties of three isomeric pentenes. *Journal of the American Chemical Society* **1949**, 71 (8), 2767-2773.
- (87) Johnson, R. Computational chemistry comparison and benchmark database, nist standard reference database 101. *National Institute of Standards and Technology* **2002**.
- (88) Dorofeeva, O. V. Ideal gas thermodynamic properties of oxygen heterocyclic compounds Part 1. Three-membered, four-membered and five-membered rings. *Thermochimica Acta* **1992**, 194, 9-46.
- (89) Gurvich, L. V.; Veyts, I. *Thermodynamic Properties of Individual Substances: Elements and Compounds*; CRC press, 1990.
- (90) Frenkel', M. L. v. *Thermodynamics of organic compounds in the gas*



state; CRC press, 1994.

(91) Yagi, K.; Keçeli, M.; Hirata, S. Optimized coordinates for anharmonic vibrational structure theories. *The Journal of Chemical Physics* **2012**, *137* (20), 204118.

(92) Barton, D.; Head, A.; Williams, R. 452. The kinetics of the dehydrochlorination of substituted hydrocarbons. Part VIII. The mechanisms of the thermal decompositions of n-propyl and n-butyl chloride and 2:2'-dichlorodiethyl ether. *Journal of the Chemical Society (Resumed)* **1951**, 2039-2046.

(93) Garcia de Sarmiento, M. A.; Dominguez, R. M.; Chuchani, G. Electronic effects of polar substituents at the acyl carbon. The pyrolysis kinetics of several isopropyl esters. *The Journal of Physical Chemistry* **1980**, *84* (20), 2531-2535.

(94) Chuchani, G.; Triana, J. L.; Rotinov, A.; Caraballo, D. F. Gas-phase elimination kinetics of ethyl esters of chloroacetate, 3-chloropropionate, and 4-chlorobutyrate. The electronic effects of substituents at the acyl carbon. *The Journal of Physical Chemistry* **1981**, *85* (9), 1243-1245.

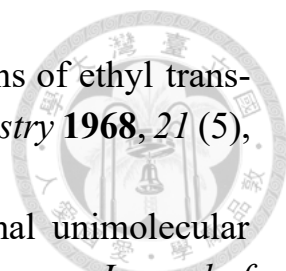
(95) Martin, G.; Roper, M.; Avila, R. Gas-phase thermolysis of sulfur compounds. Part V. Methyl allyl, diallyl and benzyl allyl sulfides. *Phosphorus and Sulfur and the Related Elements* **1982**, *13* (2), 213-220.

(96) Chuchani, G.; Rotino, A.; Martin, I.; Avila, I.; Dominguez, R. M. Influence of polar. alpha.-substituents in the gas-phase pyrolysis kinetics of tertiary chlorides. Correlation of alkyl and polar groups. *The Journal of Physical Chemistry* **1985**, *89* (19), 4134-4137.

(97) Chuchani, G.; Martin, I.; Yopez, M.; Diaz, M. Kinetics of the gas-phase pyrolysis of some secondary acetates. *Reaction Kinetics and Catalysis Letters* **1977**, *6*, 449-454.

(98) de Burgh Norfolk, S.; Taylor, R. The mechanism of the gas-phase pyrolysis of esters. Part IV. Effects of substituents at the β -carbon atom. *Journal of the Chemical Society, Perkin Transactions 2* **1976**, (3), 280-285.

(99) August, R.; McEwen, I.; Taylor, R. The mechanism of thermal eliminations. Part 22. Rate data for pyrolysis of primary, secondary, and tertiary β -hydroxy alkenes, β -hydroxy esters, and β -hydroxy ketones. The dependence of transition-state structure for six-centre eliminations upon compound type. *Journal of the Chemical Society, Perkin Transactions 2* **1987**, (11), 1683-1689.

- 
- (100) Kairaitis, D.; Stimson, V. The thermal decompositions of ethyl trans-crotonate and ethyl n-butyrate. *Australian Journal of Chemistry* **1968**, *21* (5), 1349-1354.
- (101) Barnard, J. A.; Cocks, A. T.; Parrott, T. K. Thermal unimolecular decomposition of ethyl propionate behind reflected shock waves. *Journal of the Chemical Society, Faraday Transactions 1: Physical Chemistry in Condensed Phases* **1976**, *72*, 1456-1463.
- (102) Heydtmann, H.; Dill, B.; Jonas, R. The thermal unimolecular decompositions of C₂H₅Cl, i-C₃H₇Cl, and t-C₄H₉Cl. *International Journal of Chemical Kinetics* **1975**, *7* (6), 973-979.
- (103) King, K. D. Very low-pressure pyrolysis (VLPP) of 3-chloropropionitrile. *Journal of the Chemical Society, Faraday Transactions 1: Physical Chemistry in Condensed Phases* **1978**, *74*, 912-918.
- (104) Grimme, S. Supramolecular binding thermodynamics by dispersion-corrected density functional theory. *Chemistry—A European Journal* **2012**, *18* (32), 9955-9964.
- (105) Eder, F.; Stockenhuber, M.; Lercher, J. Brønsted acid site and pore controlled siting of alkane sorption in acidic molecular sieves. *The Journal of Physical Chemistry B* **1997**, *101* (27), 5414-5419.
- (106) Malloum, A.; Conradie, J. Adsorption free energy of phenol onto coronene: Solvent and temperature effects. *Journal of Molecular Graphics and Modelling* **2023**, *118*, 108375.
- (107) Chen, W.; Zhang, P.; Truhlar, D. G.; Zheng, J.; Xu, X. Identification of Torsional Modes in Complex Molecules Using Redundant Internal Coordinates: The Multistructural Method with Torsional Anharmonicity with a Coupled Torsional Potential and Delocalized Torsions. *Journal of Chemical Theory and Computation* **2022**, *18* (12), 7671-7682.
- (108) Ghale, S. B.; Lanorio, J. G.; Nickel, A. A.; Ervin, K. M. Conformational Effects on Gas-Phase Acidities of Isomeric C₃ and C₅ Alkanols. *The Journal of Physical Chemistry A* **2018**, *122* (39), 7797-7807.
- (109) Chuchani, G.; Martin, I.; Yopez, M.; Díaz, M. Kinetics of the gas-phase pyrolysis of some secondary acetates. *React. Kinet. Catal. Lett.* **1977**, *6* (4), 449-454.
- (110) Barton, D.; Head, A.; Williams, R. 452. The kinetics of the dehydrochlorination of substituted hydrocarbons. Part VIII. The mechanisms of the thermal decompositions of n-propyl and n-butyl chloride and 2: 2' -

dichlorodiethyl ether. *J. Chem. Soc.* **1951**, 2039-2046.

(111) Choo, K. Y.; Golden, D. M.; Benson, S. W. Very low-pressure pyrolysis (VLPP) of t-butylmethyl ether. *Int. J. Chem. Kinet.* **1974**, 6 (5), 631-641.

(112) Chuchani, G.; Hernandez, J. A. Kinetics of the unimolecular elimination of chlorobutanones in the gas phase. *J. Phys. Chem.* **1981**, 85 (26), 4139-4141.

(113) Guirgis, G. A.; Drew, B.; Gounev, T.; Durig, J. Conformational stability and vibrational assignment of propanal. *Spectrochimica Acta Part A: Molecular and Biomolecular Spectroscopy* **1998**, 54 (1), 123-143.

(114) Crowder, G. Vibrational and conformational analysis of 2-methyl-1-butene. *Spectroscopy letters* **1993**, 26 (10), 1923-1938.

(115) Shimanouchi, T. *Tables of molecular vibrational frequencies*; National Bureau of Standards Washington, DC, 1972.

(116) Sverdlov, L.; Kovner, M.; Krainov, E. *Vibrational Spectra of Polyatomic molecules*, (Israel Program for Scientific Translations). J. Wiley & Sons: New York, Toronto: 1974.